The spectral radiance of indirectly illuminated surfaces in regions of permanent shadow on the Moon

P.G. Lucey[1], P.O. Hayne[2], E.S. Costello[1*], R. Green[3], C.A. Hibbitts[4], A. Goldberg[4], E. Mazarico[5], S. Li[1], C. Honniball[5]

*Corresponding Author: E.S. Costello, ecostello@higp.hawaii.edu

1. Hawaii Institute of Geophysics and Planetology, Honolulu, HI
2. University of Colorado, Boulder, CO
3. NASA Jet Propulsion Laboratory, California Institute of Technology, Pasadena, CA
4. Johns Hopkins University Applied Physics Laboratory, Laurel, MD
5. NASA Goddard Space Flight Center, Greenbelt, MD

Abstract

Regions of permanent shadow at the lunar poles have been suggested to host water ice and potentially other volatile compounds owing to their extremely low temperatures. Imaging in permanent shadow using indirect lighting from nearby topographic highs illuminated by the Sun has demonstrated the feasibility of optical remote sensing of permanent shadow surfaces, and a near-IR detection of water ice spectral features demonstrates the ability to collect usable spectroscopic data. The infrared emission of the lunar surface is largely in radiative equilibrium, so the temperature of surfaces in permanent shadow is driven by the intensity of the indirect illumination. This means that surfaces at very low temperatures, of high interest owing to their ability to trap and retain volatile compounds, will be the most challenging to measure.

We provide estimates of indirect spectral radiance as a function of permanent shadow temperature from 400 nm to 14 microns using empirical data on permanent shadow temperature and broadband visible and near IR radiance, coupled with known reflectance properties of lunar materials. The relationships show there is ample radiance and photon radiance for reflectance imaging and spectroscopy from 400nm to 8 microns at PSR temperatures above 60K with appropriately designed instruments. Beyond 8 microns lunar spectral properties reduce the available radiance substantially, making reflectance observations challenging.

Introduction

Regions of permanent shadow at the poles of the Moon are of extremely high interest at present owing to the potential for water ice to be a crucial resource for exploration of space. Permanently shadowed regions (PSR) occur at the lunar poles because the tilt of the Moon's rotation axis with respect to its path around the Sun is so small (1.5 degrees) that topographic depressions near the poles, such as the many impact craters, can be permanently shaded. The lack of direct solar illumination allows lunar surfaces within permanent shadow to achieve extremely low temperatures; surfaces at 35 Kelvin have been detected using data from a

sensitive radiometer in lunar orbit (Paige et al. 2010). These low temperature surfaces can act as cold traps, collecting volatile compounds that may circulate in the lunar environment, including water and other species (Watson et al. 1961).

At very low temperatures, solar system ices are efficiently cold trapped and resistant to losses from sublimation. The sublimation rate is exponentially dependent on temperature so there is a relatively sharp temperature cutoff between a surface that can retain an ice for geologic time, and a slightly warmer one that would allow the ice to sublimate quickly. In the case of water ice, at 100K a layer of ice about 1 mm thick would persist for a billion years against sublimation, whereas at 125K, the approximate maximum temperature for a PSR, the same layer would be lost in about 10,000 years (Zhang and Paige, 2009). At sufficiently low temperatures for any ice, other loss mechanisms are present and will dominate over sublimation, including erosion from interplanetary UV radiation, solar wind sputtering and micrometeorites (Farrell et al. 2019), but low temperatures are a necessary if insufficient condition for preservation of an ice deposit over geologic time.

While these PSR surfaces are shaded from direct illumination, many portions of permanent shadow are indirectly lit by nearby topographic highs that are illuminated by the Sun during favorable times of the lunar day and seasons. For example, the floor of a shadowed crater can receive light reflected from the sunlit upper wall of the crater (**Figure 1**). This indirect lighting has been exploited to conduct imaging of surfaces in permanent shadow using highly sensitive cameras that can take advantage of this dim illumination (Haruyama et al. 2013; Speyerer and Robinson, 2013).

When present, indirect lighting controls the temperature of the surface in permanent shadow as the Moon's highly insulating regolith surface is in radiative equilibrium with its environment. The result is that the low temperatures of the PSRs vary throughout the lunar day depending on the availability of indirect lighting. Because of the dominance of indirect lighting on temperature, the most favorable lighting conditions for imaging will also tend to be the highest temperature conditions.

This correlation of temperature and indirect illumination raises the issue that some of the most interesting portions of PSR regions, those that can preserve water and other ices against sublimation, will be the most challenging for imaging, and especially for spectroscopic measurements that finely divide available light into small wavelength bins.

In this paper we will quantify the correlation of PSR temperature and indirect lighting in order to use temperature to predict the light available for PSR imaging and spectroscopy. PSR temperatures at a wide range of lunar time of day and season have recently been made available that can be used as the input for this prediction (Williams et al. 2019). We will also show that a significant amount of light is available from thermal emission from sunlit surfaces that can be used for

imaging or reflectance spectroscopy to about 9 microns. The bases of this prediction are simultaneous measurements of temperature and solar reflected radiance in PSRs provided by the Diviner Lunar Radiometer Experiment (Paige et al. 2010) that clearly reveal the correlation of indirect illumination and temperature. These measurements also reveal via modeling that indirect solar illumination alone cannot account for the observed temperatures; the infrared emission from the illuminated surface must be included, and is roughly equal in total intensity to the illumination from reflected sunlight.

We will produce model spectral radiance curves for PSR surfaces as a function of temperature that will be useful for experiment designers, and use a simple and optimistic point design for a spectrometer to show the relationship between surface temperature and signal to noise ratio with wavelength for reasonable instrument parameters.

Data

The Diviner Lunar Radiometer on the Lunar Reconnaissance Orbiter is a nine-channel radiometer that has operated since July, 2009. Diviner's two solar channels, which both span 0.3 to 3 μm, are used to measure the reflected solar radiation as an input to understanding the thermal properties of the Moon. Diviner's longer wavelength thermal infrared channels span the mid- to far-infrared between 13 and 400 μm and are used to understand the Moon's thermal environment and thermophysical properties. In this paper data from the first year of operation that passed repeatedly over the south polar crater Shackleton, resulting in many repeat observations with the solar and thermal bands.

Solar Radiance and Surface Temperature Relationships

Figure 2 plots PSR temperatures from Diviner's 50-100 micron channel against radiance from the Diviner solar channel for repeated observations of Shackleton crater at the lunar South Pole. A clear correlation is present between the surface temperature and the solar radiance reflected, albeit a nonlinear correlation, strongly indicating the dominance of the surface temperature by radiative equilibrium.

We model this relationship by relating the temperature of the PSR surface to the reflected irradiance that governs that temperature using the equation of radiative equilibrium

$$I(1 - A) = \epsilon\sigma {T_{psr}}^4 \qquad \text{eq 1}$$

where I is the irradiance (watts/m2) that falls on the surface to drive the temperature, A is the albedo (the irradiance not reflected is absorbed by the surface and contributes to heating) and emissivity is the efficiency by which a surface can emit its radiation.

The light reflected from the surface is the radiance measured by Diviner and is related to the irradiance that illuminates the surface by:

$$L_{<3um} = \frac{I_{<3um} A_{<3um}}{\pi} \quad \text{eq 2}$$

Where the subscript "< 3um" refers to the bandpass of the Diviner "solar channel." These data are so denoted as though the bandpass is actually 0.4 to 3 microns. We note there is a small portion of UV radiation that contributes to heating that is not captured by Diviner's Channel 1, and the infrared emission solid angle in the bottom of craters is slightly less than π steradians, being slightly limited by the walls of the craters themselves.

Solving equation 2 for irradiance

$$I_{<3um} = \frac{\pi L_{<3um}}{A_{<3um}} \quad \text{eq 3}$$

we can combine equations 1 and 3 to directly relate Diviner channel 1 measurements to measured temperature, in this case assuming the temperature is governed by the < 3um irradiance

$$L_{<3um} = \frac{A_{<3um}}{\pi(1-A_{<3um})} \epsilon\sigma {T_{psr}}^4 \quad \text{eq 4}$$

The results are shown in **Figure 2**. Using nominal values for albedo of 0.16 and emissivity of 0.98 used by Vasavada et al. (2012) to match the global properties of the illuminated Moon, the estimated temperature is too low: not enough energy is absorbed by the surface. Lowering the albedo to 0.09 provides a good match to the data. However, the floor of Shackleton is known to be unusually reflective for lunar materials as measured by its normal albedo at 1064 nanometers (Lucey et al. 2014). Compared to other craters of its size, its floor is among the most reflective of the entire population, and this high reflectance has even been used to justify an interpretation of exposed ice in its interior (Zuber et al. 2012). Using a more realistic value of albedo of 0.2, the model temperature is even lower, by on the order of 20 degrees. Thus there is a missing irradiance source, and that source is thermal emission from the nearby illuminated surfaces.

We revise the model to include thermally emitted irradiance from the illuminated surroundings.

$$I_{<3um}(1 - A_{<3um}) + I_{>3um}(1 - A_{>3um}) = \epsilon\sigma {T_{psr}}^4 \quad \text{eq 5}$$

The infrared reflected radiance is not measured by Diviner (its three bands near 8 microns are narrow and lack the sensitivity to measure the PSR reflectance), but with reasonable assumptions we can model that reflected light.

Rearranging equation 5 and including Eq. 3 we arrive at:

$$I_{>3um} = \frac{\epsilon\sigma {T_{psr}}^4 - \frac{\pi L_{<3um}}{A_{<3um}}(1-A_{<3um})}{1-A_{>3um}} \quad \text{eq 6}$$

Note that In the thermal region the irradiance from emission couples into the surface with the infrared albedo, rather than the visible albedo. Most of the thermal emission from illuminated surfaces emits its energy beyond 9 microns where the albedo of the Moon is quite low, and so must be treated separately from the solar region albedo.

To determine the relative contribution of wavelengths less than and greater than 3 microns, we plot in **Figure 3** the >3um irradiance from equation 6, relative to the total (found by summing $I_{>3um}$ from eq 6 and $I_{<3um}$ from eq 3). For the PSR solar reflectance we use 0.2 and for the infrared reflectance 0.05. The value of the ratio is about 0.57, meaning that just over half the irradiance responsible for Shackleton's PSR temperatures arises from thermal emission from the crater's walls.

Is this reasonable? The energy leaving the illuminated surface is partitioned between the visible and infrared, its total being driven by the solar region (< 3um) albedo and solar irradiance and must be in balance as the lunar surface is largely in radiative equilibrium. The ratios of the solar and thermal irradiances to the total are controlled by the albedo of the surface providing the illumination.

$$\frac{I_{<3um,PSR}}{I_{>3um,PSR}+I_{<3um,PSR}} = A_{wall,<3um} \quad \text{eq 8}$$

and

$$\frac{I_{>3um,PSR}}{I_{>3um,PSR}+I_{<3um,PSR}} = 1 - A_{wall,<3um} \quad \text{eq 9}$$

The IR/total ratio of 0.57 requires a visible albedo of 1 minus that value, or 0.43, With that value, 43% of the incident solar illumination will be reflected, and 57% absorbed and promptly re-emitted as thermal radiation.

Forty three percent may appear to be a very high reflectance, especially with respect to the 0.16 assumed by Vasavada et al. for the global Moon. However, Shackleton's walls are unusually reflective, like its floor, and is known to be composed of an highly reflective mineral, the alumino-silicate plagioclase (Haruyama et al. 2013). Furthermore the global Moon value is low in part because of the darkening that accompanies exposure of lunar surface materials (Fischer and Pieters, 1996), whereas the walls of Shackleton are constantly renewed by mass wasting (movement of material downslope exposing material not influenced by exposure to space).

We can test this albedo estimate with direct Diviner temperature measurements of the walls of Shackleton, because the albedo, together with the angle of the Sun with respect to Shackleton's wall, drive the wall temperature.

$$cos(i)(1 - A_{wall})I_{solar} = \epsilon\sigma {T_{wall}}^4 \quad \text{eq 10}$$

At south polar Shackleton crater, the Sun is always at a near grazing angle to the average surface. Shackleton's illuminated walls are inclined toward the Sun by about 30 degrees, so the solar incidence angle is about 60 degrees. Using this angle, the solar constant of 1360 watts/m^2 for normal incidence at 1 AU for I_{solar}, and 43% albedo for the wall, gives a radiative equilibrium temperature of 291K for Shackleton's wall. Direct Diviner measurements of the maximum temperatures of the walls of Shackleton range from 280 to over 290K (**Figure 4**); this supports the assignment of a 43% albedo to the Shackleton wall, and supports the estimated partitioning of solar reflected and lunar emitted light into Shackleton's PSR.

The final model to predict the radiance of the PSR surfaces at both solar (<3um) and infrared (> 3um) wavelengths from temperature is then derived from equation 5, where $I_{<3um}$ and $I_{>3um}$ are related by radiative balance which is represented by equations 8, 9 and 10.

The ratio of eqs. 8 and 9 relate the PSR irradiances to the wall albedo and is written:

$$\frac{I_{<3um,PSR}}{I_{>3um,PSR}} = \frac{A_{wall,<3um}}{1-A_{wall,<3um}} \qquad \text{eq 11}$$

allowing solutions to relate irradiance to temperature for the solar and infrared bands separately by substitution into equation 5 using the relationship in eq 11:

$$I_{>3um,PSR}\frac{A_{wall,<3um}}{1-A_{wall,<3um}}\left(1-A_{<3um,PSR}\right) + I_{>3um}\left(1-A_{>3um,PSR}\right) = \epsilon\sigma {T_{psr}}^4 \quad \text{eq 12}$$

which relates the >3um irradiance and temperature without involving the <3um irradiance, and

$$I_{<3um}(1-A_{<3um}) + I_{<3um,PSR}\frac{1-A_{wall,<3um}}{A_{wall,<3um}}(1-A_{>3um}) = \epsilon\sigma {T_{psr}}^4 \quad \text{eq 13}$$

relates the <3um irradiance and temperature without involving the >3um irradiance.

Solving eqs 12 and 13 for $I_{>3um,psr}$ and $I_{<3um,psr}$ respectively results in:

$$I_{>3um,PSR} = \frac{\epsilon\sigma {T_{psr}}^4}{\left[\left(1-A_{>3um,PSR}\right)+\frac{A_{wall,<3um}}{1-A_{wall,<3um}}\left[\left(1-A_{<3um,PSR}\right)\right]\right]} \qquad \text{eq 14}$$

and

$$I_{<3um} = \frac{\epsilon\sigma {T_{psr}}^4}{\left[\left(1-A_{PSR,<3um}\right)+\frac{1-A_{wall,<3um}}{A_{wall,<3um}}\left(1-A_{PSR,>3um}\right)\right]} \qquad \text{eq 15}$$

We can calculate $L_{<3um}$ and $L_{>3um}$ using eqs 14 and 15 by recalling the relationship between reflected light and irradiance presented in eq 2. The result gives the

radiance reflected from the surface (L) as a function of the albedos (A) and temperature (T) in each band.

$$L_{>3um,PSR} = \frac{A_{>3um,PSR}}{\pi} \frac{\epsilon\sigma {T_{psr}}^4}{\left[(1-A_{>3um,PSR}) + \frac{A_{wall,<3um}}{1-A_{wall,<3um}}[(1-A_{<3um,PSR})]\right]} \quad \text{eq 16}$$

and

$$L_{<3um} = \frac{A_{<3um,PSR}}{\pi} \frac{\epsilon\sigma {T_{psr}}^4}{\left[(1-A_{<3um}) + \frac{1-A_{wall,<3um}}{A_{wall,<3um}}(1-A_{>3um})\right]} \quad \text{eq 17}$$

As the albedos in the above equations are all constants, these equations can be simplified using the values in **Table 1**

$$L_{band} = K_{band}\epsilon\sigma {T_{psr}}^4 \quad \text{eq 18}$$

where "band" is visible-near-IR (< 3um) or IR (> 3um).

Table 1 lists three cases: a bright PSR such as Shackleton, a nominal PSR where the surfaces are somewhat brighter than typical lunar surfaces as determined by laser reflectance (Lucey et al. 2014), and the lunar typical case used by Vasavada et al. 2012. For the purposes of first order calculations, there is little difference between the PSR nominal and lunar typical cases, only the highly anomalous Shackleton case is significantly different (and for those not familiar with south polar lunar geology, there are no anomalously dark surfaces in the lunar polar regions at the 1 km or greater scale as demonstrated by laser reflectance maps of surface albedo (Fisher et al. 2017).

Illuminated wall solid angle

For some researchers the reaction of the PSR floor temperature to the illuminated area of wall exposed may be of interest. The solid angle of the illuminated wall is related to the total irradiance of the PSR by:

$$I_{total,PSR} = L_{wall}\Omega_{wall}\cos(i_{wall}) \quad \text{eq 19}$$

where i_{wall} is the angle between the surface normal of the PSR and the illuminating wall.

Rearranging equation 3, we solve for the PSR irradiance.

$$I_{<3um,PSR} = L_{<3um}\frac{\pi}{A_{<3um,PSR}} \quad \text{eq 20}$$

However, the total power incident when the infrared is included is about double the <3um power as discussed above, so:

$$I_{total,PSR} = 2L_{<3um}\frac{\pi}{A_{<3um,PSR}} \quad \text{eq 21}$$

Equating the right sides of eq 19 and 21 we can relate the solid angle and the measured Diviner solar channel radiance

$$2L_{<3um}\frac{\pi}{A_{<3um,PSR}} = L_{wall}\Omega_{wall}\cos(i_{wall}) \qquad \text{eq 22}$$

and, solving for Ω_{wall} gives:

$$\Omega_{wall} = \frac{2\pi L_{<3um}}{A_{<3um,PSR}L_{wall}\cos(i_{wall})} \qquad \text{eq 23}$$

The total radiance of the wall is given by

$$L_{wall} = \frac{\cos i_{sun} I_{solar}}{\pi} \qquad \text{eq 24}$$

where I_{solar} is the solar irradiance, and i_{sun} is the solar incidence angle on the illuminated wall. There is no albedo term because in equilibrium any light not reflected is absorbed and is re-emitted in the infrared.

We replace L_{wall} with the form in eq 24 so that:

$$\Omega_{wall} = \frac{2\pi L_{<3um}}{A_{<3um,PSR} I_{solar} \cos i_{sun} \cos(i_{wall})} \qquad \text{eq 25}$$

And since $L_{<3um}$ can be predicted from temperature by eq 18:

$$\Omega_{wall} = \frac{2\pi K_{<3um}\epsilon\sigma {T_{psr}}^4}{A_{<3um,PSR} I_{solar} \cos i_{sun} \cos(i_{wall})} \qquad \text{eq 26}$$

For Shackleton, $A_{<3um,PSR} = 0.2$, $i_{sun} = 60$, i_{wall}=20, and $K_{<3um}$ = 0.032. **Figure 5** shows the solid angle subtended by the wall as a function of PSR temperature for the Shackleton case. For context, to result in a 100K PSR temperature in the center of the floor of Shackleton, which is situated ten kilometers from the rim, an area of the upper wall 2 km^2 must be illuminated. This is equivalent to a strip of wall 10 km long and 200 m high which is a reasonable approximation of typical illumination at this crater (**Figure 1**).

For further context, the Earth has about the same radiance as the illuminated wall of Shackleton (similar visible albedoes and temperature). From the Moon the Earth subtends a solid angle of about 3x10^{-3} steradians and for some PSR surfaces the Earth can be fully in the field of view, low on the horizon. **Figure 5** shows that this solid angle subtended by source with the same radiance properties as the Shackleton wall would drive the surface temperature to 60K, and provide illumination for imaging and spectroscopy. As Glenar et al. 2019 pointed out, there is ample illumination for broadband imaging using Earthshine. Because Earthshine is at its maximum on the lunar nightside, it opens up the availability of PSR surfaces for measurement. However, Earth exhibits very strong spectral features that may compete with spectral features of materials of interest within PSR and possibly cause false detections. The solid angle of the Earth relative to illuminated surfaces should be taken into account when interpreting high precision spectral data, even

on the lunar day side where illumination is dominated by indirect lighting from lunar sunlit surfaces.

PSR Spectral radiance

The spectacular images of the interior of Shackleton crater of Haruyama et al. 2013, and other PSR by Robinson et al. 2013 have demonstrated that for many PSR there is sufficient light for broadband imaging, at least at favorable times of the lunar day. Moreover, Li et al. 2018 showed that reflectance spectroscopy is possible in PSR by detecting ice bands near 1.25, 1.5 and 1.9 microns, though that experiment required extensive data averaging to tease out a signal. The calculations above, with modest assumptions, allow the estimation of the reflected spectral radiance as a function of PSR temperature, useful for experiment design for existing instruments in lunar polar orbit and for planned or contemplated experiments.

The spectral radiance is the wavelength dependent power departing a surface, normalized to unit solid angle, area and spectral bandpass. This quantity is a critical input for assessing the potential performance of spectral sensors that feature bands narrower than the wide 400-3000 nm and > 3000nm bands considered above. That there is reflected solar illumination is obvious, and was exploited by the experiments discussed above. However, we have shown that the thermal emission from the illuminated crater walls or other topographic highs bathes the interior of PSRs in substantial illumination between 3 and about 14 microns, as this is the range of peak emission for the approximately 300K temperatures of lunar features illuminated by the Sun in the polar regions. This infrared illumination is potentially enabling of experiments seeking infrared spectral features that may not have been previously considered, such as CO_2, ammonia and methane ice or adsorbates, organics, molecular water and the signatures of silicate minerals.

The spectral irradiance on the PSR surface is related to the radiance of the wall, its spectral reflectance or emission, the solid angle of the wall as viewed by the PSR surface, and the average angle of the incidence of the wall illumination (i_{wall}) (see eq 20).

Adapting eq 2 to the spectral case, in the <3um band the wall spectral radiance is modeled as:

$$L_{<3um,\lambda,wall} = \frac{I_{solar,\lambda}\,\phi R_{wall,\lambda}}{\pi} \qquad \text{eq27}$$

where all variables are wavelength dependent, phi is a photometric function and R is the spectral reflectance of the illuminated wall and I_{solar} is the solar spectral irradiance.

In the IR (>3um) , we model the wall radiance as:

$$L_{>3um,\lambda,wall} = B(T_{wall})(1 - R_{wall,\lambda}) \qquad \text{eq 28}$$

where B(T) is the Planck function. The relationship between reflectance and emissivity assumes Kirchoff's Law (1=R+ε) is valid. As noted below, this relationship does not hold beyond 9 microns.

The irradiances on the PSR resulting from the wall radiances are given by equation 19 adapted to the spectral case.

$$I_{<3um,\lambda,psr} = \frac{\Omega_{wall} I_{solar,\lambda}\, \Phi_{wall} R_{wall,\lambda}}{\pi} \quad \text{eq 29}$$

$$I_{>3um,\lambda,psr} = \Omega_{wall} B(T_{wall})(1 - R_{wall,\lambda}) \quad \text{eq 30}$$

The irradiance is then multiplied by the floor spectrum in either the IR or visible and normalized by π to derive the PSR radiance. This model can include more complex photometric functions, but for the purposes here, the cos(i) relationship, which assumes pure Lambertian behavior, is sufficient as shown in the next section.

$$L_{<3um,\lambda,psr} = \frac{\Omega_{wall}\Phi_{wall}\Phi_{PSR} I_{solar,\lambda}\, R_{wall,\lambda} R_{PSR,\lambda}}{\pi^2} \quad \text{eq 31}$$

$$L_{>3um,\lambda,psr} = \frac{\Omega_{wall}\Phi_{PSR} B(T_{wall})(1-R_{wall,\lambda}) R_{PSR,\lambda}}{\pi} \quad \text{eq 32}$$

This spectral radiance, when integrated over wavelength, must be equal to the total radiance measured by Diviner or estimated from Diviner in each of the two bands.

$$L_{<3um,psr} = \int_{0.4}^{3} L_{\lambda,<3um,psr} \quad \text{eq 33}$$

$$L_{>3um,psr} = \int_{3}^{\infty} L_{\lambda,>3um,psr} \quad \text{eq 34}$$

Because of this known constraint, the spectral radiance can be normalized over that band and set equal to the Diviner measurement, so the nominally constant terms--Ω and photometric function functions needed to determine absolute irradiance and radiance--cancel, and only the spectrally varying terms need be included.

So the spectral radiance of the PSR surface is the sum of the solar and thermal emission inputs

$$L_{\lambda,PSR} = L_{<3um} \frac{I_{solar,\lambda} R_{wall,\lambda} R_{PSR,\lambda}}{\int_{.4}^{3} I_{solar,\lambda} R_{wall,\lambda} R_{PSR,\lambda}} + L_{>3um} \frac{B(T_{wall})(1-R_{wall,\lambda}) R_{PSR,\lambda}}{\int_{3}^{\infty} B(T_{wall})(1-R_{wall,\lambda}) R_{PSR,\lambda}} \quad \text{eq 35}$$

where L_{band} is from eq 18 and **Table 1**, and a temperature of 286 for T_{wall} is reasonable.

For the models shown below we use the solar irradiance curve of ASTM International (2008) for $I_{\lambda,solar}$. The solar reflectance beyond 4 microns is not reported, so we compute a 5800K blackbody and scale it to the spectral irradiance values between 3 and 4 microns to estimate solar irradiance to 100 microns. For the lunar reflectance spectrum we use the spectrum of Apollo soil 62331, which is a typical soil from the lunar highlands that is likely to be similar in reflectance

properties to polar soil. For the results shown below we use this soil spectrum for both R_{wall} and R_{psr} as the minor spectral differences among soils do not dominate the results (though their common spectral characteristics have important spectral effects as discussed below).

Results

Figure 6 shows the spectral radiance for three PSR temperatures, and two examples of illuminated surfaces for context. The illuminated models (solar noon at the equator and at 85 degrees latitude) are computed from the solar spectral irradiance, divided by π, multiplied by the reflectance spectrum of the Apollo soil and the cosine of the incidence angle. For their temperature we take $380*\cos(i)^{1/4}$ which is a useful approximation of the observed infrared brightness temperature at 10 microns for nadir viewing sensors (Pettit and Nicolson, 1930), where i is the solar incidence angle. The blackbody function is multiplied by (1-R) assuming Kirchoff's Law applies.

Data are plotted in $\log_{10}$ of the radiance because of the large range in values among examples. Radiance is bimodal both on the illuminated and PSR surfaces, reflecting solar reflectance and thermal emission, but the PSR radiance is modulated by the interaction of the radiance with the lunar surface multiple times, and the greater uniformity of the shape of the thermal emission term which originates from surfaces facing the sun at 30 degrees in all cases.

The PSR temperatures plotted cover the majority of the range of maximum temperature encountered in PSRs. At the high end, shadowed surfaces adjacent to large expanses of illuminated surface show maximum temperatures of 125K, or more. At the low end, very little area in the polar regions have maximum temperatures below 60K, at least at the resolution of the Diviner data set (a scientifically important portion of the polar surface has maximum temperatures well below 60K, but these cover extremely small areas, and feature little reflected spectral radiance). 100K is an important temperature. Much above 100K, the exponential dependence of ice sublimation causes rapid loss of ice over geologically short periods [Zhang and Paige 2009]. Therefore, PSR areas with maximum temperatures between about 125 and 110K ought to be barren of ice, unless deposited extremely recently (Farrell et al. 2019). Between 60 and 100K water ice sublimation is essentially zero (at these temperatures ice loss is governed by other processes including UV erosion, solar wind ion sputtering, and most importantly, meteorite impact). It is between these 60 and 100K temperatures where surface ice is both thermally stable and there is significant surface area to explore, but indirect illumination is low.

Four orders of magnitude separate the spectral radiance available under maximum sunlit illumination conditions and a PSR at 60K, a challenge for the instrument designer. However, within PSRs the variation is about a factor of 100, and only about a factor of 10 across the critical ice temperature range of 60-100K. Within PSRs there is about an order of magnitude less spectral radiance at 7

microns compared the peak at about 500 nm in the visible, but we shall see that the decline is much less for detectors that are sensitive to the number of photons (semiconductors) as opposed to power (e.g. bolometers). The thermal emission from the surroundings has substantially filled in the available radiance near 3um which ordinarily is something of a valley of death between the peak solar irradiance and lunar thermal emission, somewhat easing the demands on instrument dynamic range.

Implications for measurements

The data shown in **Figure 6** are plotted in units of radiance, that is, watts/m2-um-sr. However, many imaging and spectroscopic instruments with semiconductor detectors are sensitive to the number of photons, not the total power. Because the number of photons per watt increases proportional to wavelength, the available signal toward the infrared is greater than implied by **Figure 6**. In **Figure 7** we show the photon radiance, that is, photons / sec-m2-um- sr. Interestingly, there are more infrared photons near their peak near 5 microns than in the visible, which is promising for potential infrared reflectance spectroscopy of PSRs. The peak emissions in the visible and infrared are near 2 and 5 microns, rather than the peaks of the illuminated Moon near 500 nm and 10 microns, due to the strong influence of lunar spectral color superimposed on the radiance curves by the two encounters with the lunar surface before departing the surface as measureable radiance (equation 35).

We also note that lunar spectral color is a complication for interpreting radiance spectra of PSRs; unlike on the illuminated surface where the Sun and inherent blackbody radiation are well known sources, the irradiance on PSR surfaces already has lunar color, and may exhibit water absorptions as well as other features of the illuminated surroundings. The problem is not insuperable, for example detection of water ice features in the near IR is not confounded by similar features on illuminated surfaces, but more subtle analyses, such as hydroxyl abundance, would have to be conducted with great care. The reference spectra used for the models presented here show water and hydroxyl features near 3 and 6 microns illustrating this issue. There is also a strong spectral feature near 8 microns, this is a spectral feature in both reflectance and emission due to a scattering minimum associated with the silicate mineralogy of the surface. We should also note that Kirchoff's Law in emission does not hold at wavelengths near and beyond 8 microns; emission is substantially lower than predicted from reflectance and the curves shown in **Figures 6** and **7** overestimate the available reflected radiance beyond 9 microns as the thermal emission source of radiance from nearby topographic highs and crater walls is likely lower than modeled beyond about 8 microns.

Implications for spectral instruments

We use a simple sensor model to estimate potential sensitivity of reflectance measurements for these PSR photon radiances. We assume a spectrographic sensor

roughly similar to the Chandrayaan-1 M3 (Pieters et al. 2009). The model instrument features 20 nm spectral resolution, and the spectrograph optics deliver an f/3 beam to the detectors. The optics have a generous 30% optical throughput and its detector uses 24 micron square pixels per spectral bin with a quantum efficiency of 70%. We integrate for 1 second in which time a spacecraft in lunar orbit will have traversed 1600 meters. Ignoring all noise sources except detected photo-electrons, the signal to noise ratios achieved by this idealized instrument are shown in **Figure 8**. Very respectable signal noise ratios are achieved, even at a PSR temperature of 60K. These sensitivities are sufficient to detect at near-IR wavelengths low abundances of water ice, near 1%, and even lower at the more absorbing 3um region.

The estimate shown in **Figure 8** is optimistic; real instruments have real noise sources. Two of these are read noise and dark current. Typical IR readout integrated circuits have read noises on the order of 500 electrons due to wide electrical bandwidths necessary for more typical short integration times and fast frame rate characteristics required by most applications, such as imaging spectroscopy of the illuminated surface. Including 500 electrons of read noise gives the result shown in **Figure 9**. Signal to noise ratios in the critical 60-100K PSR temperature range have fallen below 100, and are close to unusable near 60K. This suggests that the electrical bandwidth of common detector readouts are an important limiting factor in sensitive PSR measurements. Some sensitivity can be recovered with wider spectral bands, but at some point the spectral specificity to ice and its variations, and spectral properties of other species of interest will be lost.

Dark current, another significant source of noise, is a flow of electrons generated within the detector semiconductor due to thermal agitation and excitation within the detector itself. The electrons generated by this process cannot be distinguished from signal photo-current, and contribute noise to the measurement and consume dynamic range. A rule of thumb to minimize the contribution of dark current is to keep it less than 10% of the anticipated photocurrent from the signal source. The key to reduce dark current is to cool infrared detectors, but cooling is expensive in spacecraft resources in terms of power consumption and heat dissipation, so cooling, while necessary, is used as sparingly as possible. The dark current of mercury cadmium telluride detectors, a typical detector variety in IR spectrometers, can be estimated from an enduring empirical relationship presented by Tennant et al. 2007 informally referred to as "Rule '07" for the publication year (we assume the threshold wavelength is less than the cutoff wavelength). The photocurrent generated by our strawman spectrometer is given in **Figure 10**; our rule of thumb suggests the acceptable dark current is 1/10 this value and Rule '07 gives the temperature required to achieve it, shown in **Figure 11**. The photocurrent used in the Rule '07 calculation is for the minimum photocurrent short of the cutoff of the 60K and 100K surfaces. In this case the dark current is limited principally by the photocurrent in the 3-4 micron region. If the shortest wavelength of interest does not include these wavelengths, the dark current requirement is relaxed.

For cutoff wavelengths short of about 4 microns, required FPA temperatures are comfortably above 100K, well within the reach of modest coolers. But with increasing wavelength, cooling demands rise rapidly. For operation up to 10 microns, FPA temperatures near 50K are required, which will be stressing the technical or cost viability of the experiment for the relatively small satellites contemplated for lunar measurements. Temperatures near 70K are achievable with good satellite thermal design, which corresponds to a cutoff wavelength of about 7 microns.

Thermal emission from the spectral instrument itself can also be a significant noise source, but we elect not to model it as many creative approaches are available to mitigate this issue so a simple example may not be useful. Nevertheless, initial calculations of instrument performance in the low flux PSR situation must include this term.

Finally, the abundant flux in the infrared beyond three microns invites multispectral imaging that may target individual species with strong infrared absorption, such as carbon dioxide ice or adsorbates, organics or molecular water. These observations may profitably exploit broader bands than modeled here, and with cryogenic filters or cooled optics may mitigate instrument self-emission as a limiting noise source.

Conclusions

We produced estimates of indirect spectral radiance as a function of PSR temperature from 400 nm to 25 microns using empirical data on PSR temperature and broadband visible and near IR radiance, coupled with known reflectance properties of lunar materials. The relationships show there is ample radiance and photon radiance for reflectance imaging and spectroscopy from 400nm to 8 microns at PSR temperatures above 60K. Beyond 8 microns the very low lunar spectral albedo reduces the available radiance substantially, making reflectance observations challenging.

Earthshine provides ample illumination for imaging in PSR as pointed out by Glenar et al. 2019, and is not too faint for spectroscopic measurements. On the other hand, the spectral properties of the Earth may complicate searches for unique materials in PSR owing to its strong spectral features that will superimposed on the spectrum of the illumination.

Detector read noise is a critical limit on PSR reflectance spectroscopy; typical read noises of several hundred electrons exhibited by typical high readout rate IR imagers may prevent probing the colder parts of PSRs. Detector dark current is also important, but our simple calculations suggest spectral measurements to about 7 microns are within the reach of low cost detector cooling compatible with small lunar satellites.

Maximum temperatures within PSR, and hence maximum illumination, only occur for brief periods, often but not always near local noon in summer (Williams et

al. 2019), so a comprehensive survey of PSR spectral reflectance with high signal to noise ratios may require long mission durations as usable illumination may not be available on many orbits. Spectral sensors highly optimized for PSR measurements (low read noise, dark current and thermal emission) would allow measurements over a wider range of PSR temperatures and available lighting and reduce mission duration or increase coverage.

The available spectral radiance requires long integration times to achieve usable signal to noise ratios. For nadir facing instruments, this reduces the down-track spatial resolution achievable to kilometers, or many hundreds of meters. Image motion compensation can greatly improve the spatial resolution by increasing the dwell time on the surface, though this limits areal coverage. However, the limited spatial extent of the PSRs and the many opportunities to view them from polar orbit may allow efficient data collection strategies.

Data interpretation will be complicated by the fact that the lunar spectrum of the illuminated local topographic highs is superimposed on the PSR radiance spectrum. This light source may contain confounding spectral features of high interest within the PSR, such as absorption from hydroxyl or molecular water. However, the spectra of volatile ices are highly distinct from water-bearing lunar materials at most wavelengths except possibly at 3um where the spectral features of water or hydroxyl on the illuminated surface would complicate detection of small amounts of ice.

While typical instrument designs for lunar and planetary infrared spectroscopy are not ideal matches to spectral measurements in permanent shadow owing to the low radiances available, optimized instruments are well within current technical capabilities and require no major technological advances to achieve.

Acknowledgements

This work was funded in part by the Lunar Reconnaissance Orbiter Diviner Lunar Radiometer Experiment, David A. Paige Principal Investigator.

References

ASTM International. ASTM G173-03 (reapproved 2008), Standard Tables for Reference Solar Spectral Irradiances: Direct Normal and Hemispherical on 37° Tilted Surface. ASTM Internacional; 2008.

Farrell, W. M., 695 Hurley, D. M., Poston, M. J., Hayne, P. O., Szalay, J. R., & McLain, J. L. (2019). The Young Age of the LAMPobserved Frost in Lunar Polar Cold Traps. Geophysical Research Letters.

Fisher EA, Lucey PG, Lemelin M, Greenhagen BT, Siegler MA, Mazarico E, Aharonson O, Williams JP, Hayne PO, Neumann GA, Paige DA. Evidence for surface water ice in the lunar polar regions using reflectance measurements from the Lunar Orbiter Laser Altimeter and temperature measurements from the Diviner Lunar Radiometer Experiment. Icarus. 2017 Aug 1;292:74-85.

Glenar DA, Stubbs TJ, Schwieterman EW, Robinson TD, Livengood TA. Earthshine as an illumination source at the Moon. Icarus. 2019 Mar 15;321:841-56.

Haruyama J, Yamamoto S, Yokota Y, Ohtake M, Matsunaga T. An explanation of bright areas inside Shackleton Crater at the Lunar South Pole other than water‐ice deposits. Geophysical Research Letters. 2013 Aug 16;40(15):3814-8.).

Li S, Lucey PG, Milliken RE, Hayne PO, Fisher E, Williams JP, Hurley DM, Elphic RC. Direct evidence of surface exposed water ice in the lunar polar regions. Proceedings of the National Academy of Sciences. 2018 Sep 4;115(36):8907-12.

Lucey PG, Neumann GA, Riner MA, Mazarico E, Smith DE, Zuber MT, Paige DA, Bussey DB, Cahill JT, McGovern A, Isaacson P. The global albedo of the Moon at 1064 nm from LOLA. Journal of Geophysical Research: Planets. 2014 Jul;119(7):1665-79.

Paige DA, Siegler MA, Zhang JA, Hayne PO, Foote EJ, Bennett KA, Vasavada AR, Greenhagen BT, Schofield JT, McCleese DJ, Foote MC. Diviner lunar radiometer observations of cold traps in the Moon's south polar region. science. 2010 Oct 22;330(6003):479-82.

Pettitt, E., & Nicholson, S. R. (1930). Lunar Radiation and Temperature. Astrophys. J, 71, 102.

Pieters CM, Boardman J, Buratti B, Chatterjee A, Clark R, Glavich T, Green R, Head III J, Isaacson P, Malaret E, McCord T. The Moon Mineralogy Mapper (M^3) on Chandrayaan-1. Current Science. 2009 Feb 25:500-5.

Speyerer EJ, Robinson MS. Persistently illuminated regions at the lunar poles: Ideal sites for future exploration. Icarus. 2013 Jan 1;222(1):122-36.

Tennant WE, Lee D, Zandian M, Piquette E, Carmody M. MBE HgCdTe technology: a very general solution to IR detection, described by "Rule 07", a very convenient heuristic. Journal of electronic materials. 2008 Sep 1;37(9):1406-10.

Vasavada AR, Bandfield JL, Greenhagen BT, Hayne PO, Siegler MA, Williams JP, Paige DA. Lunar equatorial surface temperatures and regolith properties from the Diviner Lunar Radiometer Experiment. Journal of Geophysical Research: Planets. 2012 Dec;117(E12).

Watson K, Murray B, Brown H. On the possible presence of ice on the Moon. Journal of Geophysical Research. 1961 May;66(5):1598-600.

Williams JP, Greenhagen BT, Paige DA, Schorghofer N, Sefton‐Nash E, Hayne PO, Lucey PG, Siegler MA, Aye KM. Seasonal polar temperatures on the Moon. Journal of Geophysical Research: Planets. 2019 Oct;124(10):2505-21.

Zuber MT, Head JW, Smith DE, Neumann GA, Mazarico E, Torrence MH, Aharonson O, Tye AR, Fassett CI, Rosenburg MA, Melosh HJ. Constraints on the volatile distribution within Shackleton crater at the lunar south pole. Nature. 2012 Jun;486(7403):378-81

Tables

Table 1. Parameters for computing PSR radiance

	Shackleton	PSR Nominal	Lunar Typical
PSR IR albedo	0.05	0.05	0.05
PSR visible albedo	0.2	0.18	0.16
Illuminated wall albedo	0.43	0.32	0.32
K< 3um	0.036	0.022	0.019
K> 3um	0.009	0.011	0.011

Figures

Figure 1: Image of the lunar south polar Shackleton crater showing the wall of the crater illuminated by the Sun. The sunlit wall casts light, both visible and infrared, into the shadowed portion of the crater providing illumination for imaging and spectroscopy. The image is a portion of Lunar Reconnaissance Orbiter Camera, Wide Angle Camera (WAC) frame M172692029ME.

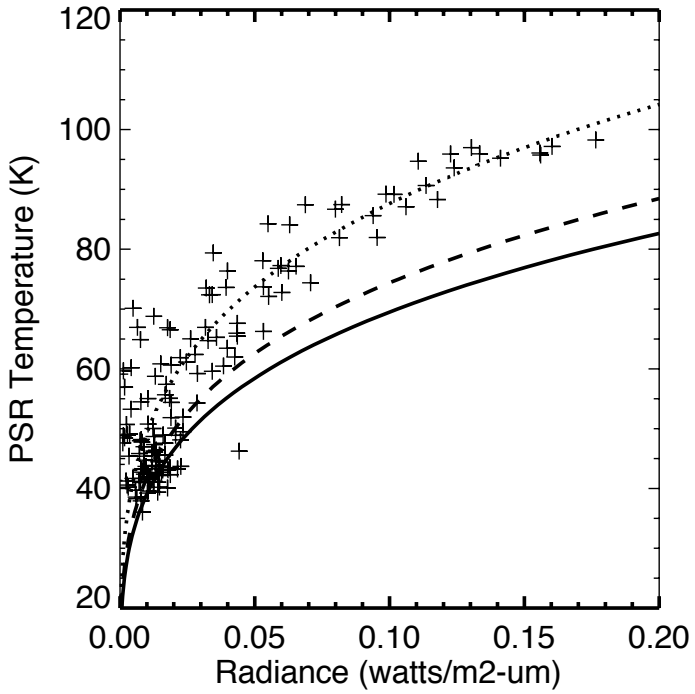

Figure 2: Crosses show data from Diviner's 50-100 micron channel against radiance from the Diviner solar channel (400nm to 3 microns) for repeated observations of the permanently shaded Shackleton crater at the lunar South Pole. The solid line plots equation 4 for an albedo of 0.2 which is representative of the floor of Shackleton. The dashed line uses a value of 0.16 which is the albedo used by Vasavada et al. () to model the global temperature behavior of the Moon from solar forcing. The dotted line is a best fit to the data using an albedo of 0.09 which is much low than the reflectance of the floor of the crater. This shows that using proper albedo values results in underprediction of temperature, showing there is unaccounted irradiance.

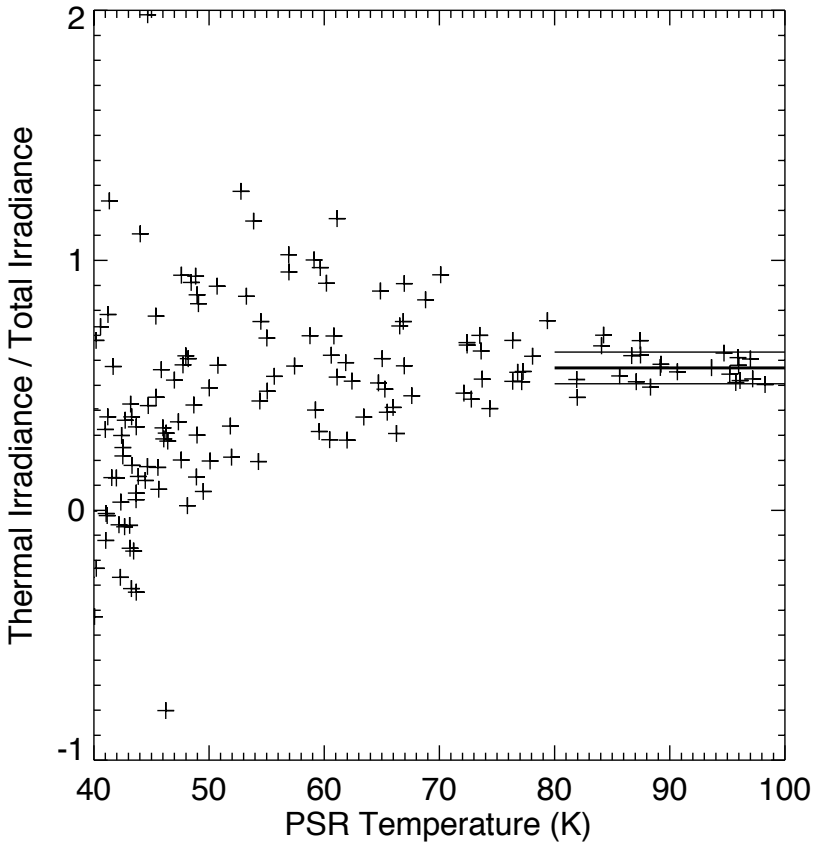

Figure 3: Model thermal irradiance originating beyond 3 microns computed from equation 6, to the total irradiance by summing the output of equations 3 and 6. The mean ratio value above 80K is 0.57. Data values flare toward lower temperatures as the surface temperature approaches the noise equivalent delta temperature and noise equivalent radiace of the radiometers.

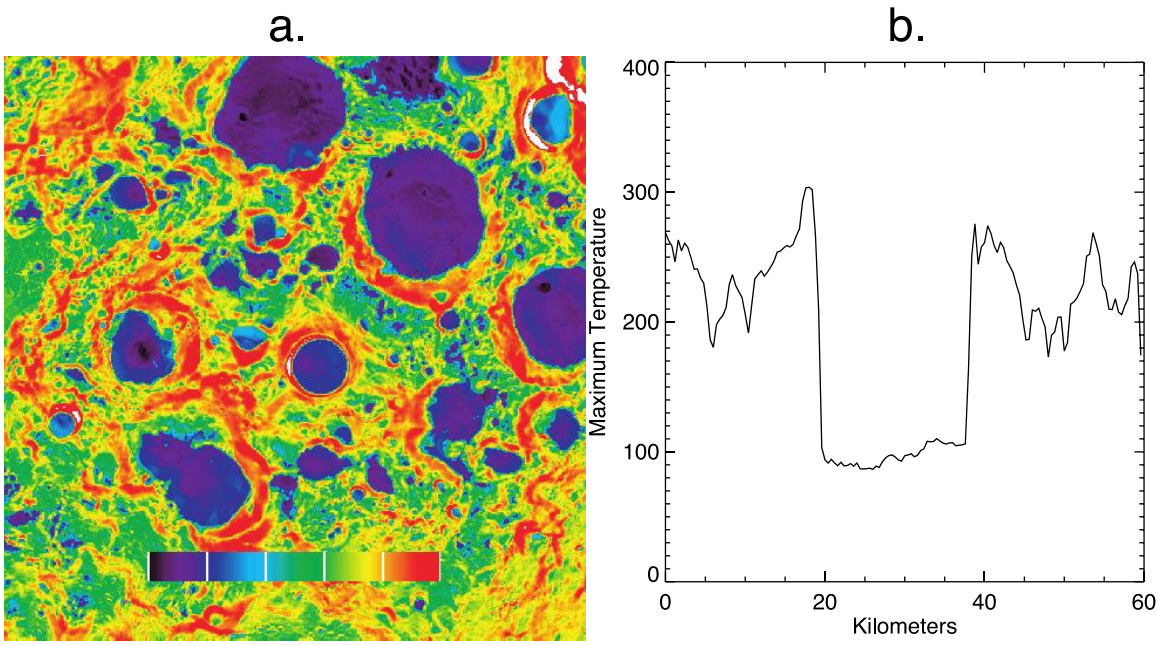

Figure 4: a. Color coded image of the maximum temperature experienced in the lunar south polar region, with the south polar crater Shackleton prominent in the center of the image. The temperatures are the maximum values recorded by the Diviner Lunar Radiometer over about ten years of operation. When sunlit, the rim of Shackleton is near 300K. b. Plot through the center Shackleton parallel to the 90 degree meridian. The direction toward the Earth is to the top.

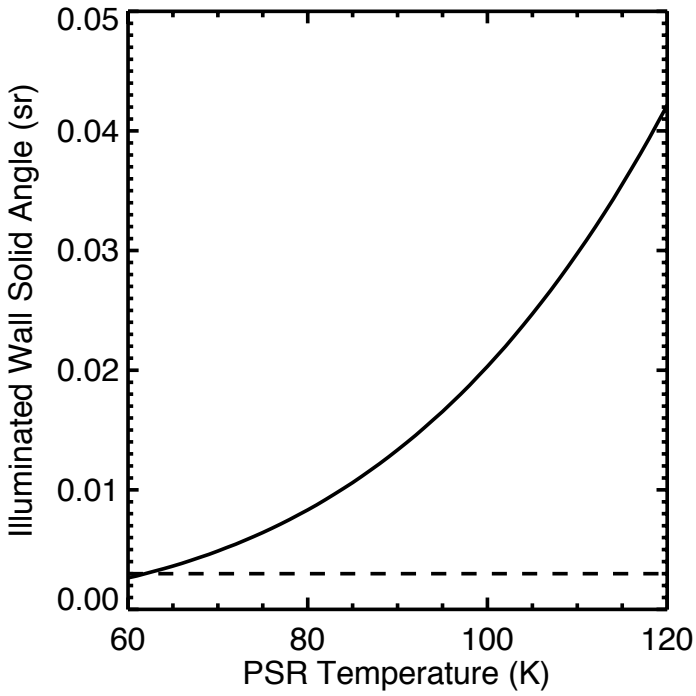

Figure 5: PSR surface temperature as a function of source solid angle driven by a source at 300K with a visible albedo of 0.2, at an angle of 20 degrees elevation. The dashed line is the solid angle of the full Earth that can be viewed by some PSR during the lunar night if situated on the near side of the Moon.

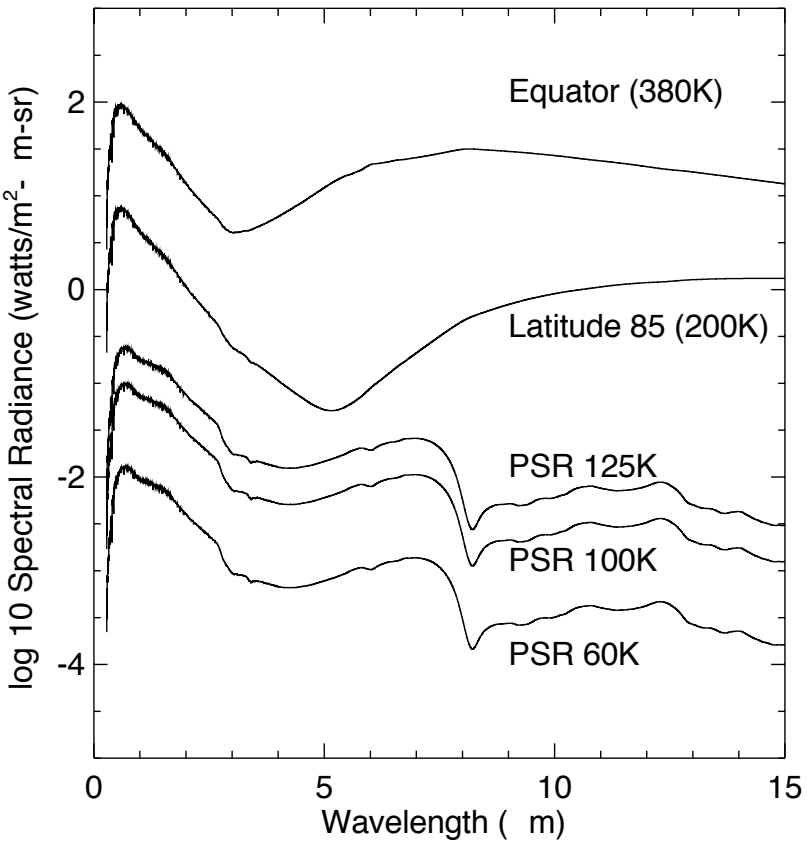

Figure 6: Lunar spectral radiance for the lunar subsolar point (top), a sunlit surface at 85 degrees latitude (second from top), and PSR surface at 125K (middle), 100K (second from bottom) and 60K (bottom). The appearance of these curves are very different because with PSR the emerging radiance has interacted with the lunar surface twice, so lunar spectral properties are more apparent. The shapes of the PSR curves are similar because the temperature is principally driven by the angle subtended by the source, and in these models the temperature of the sunlit source is constant.

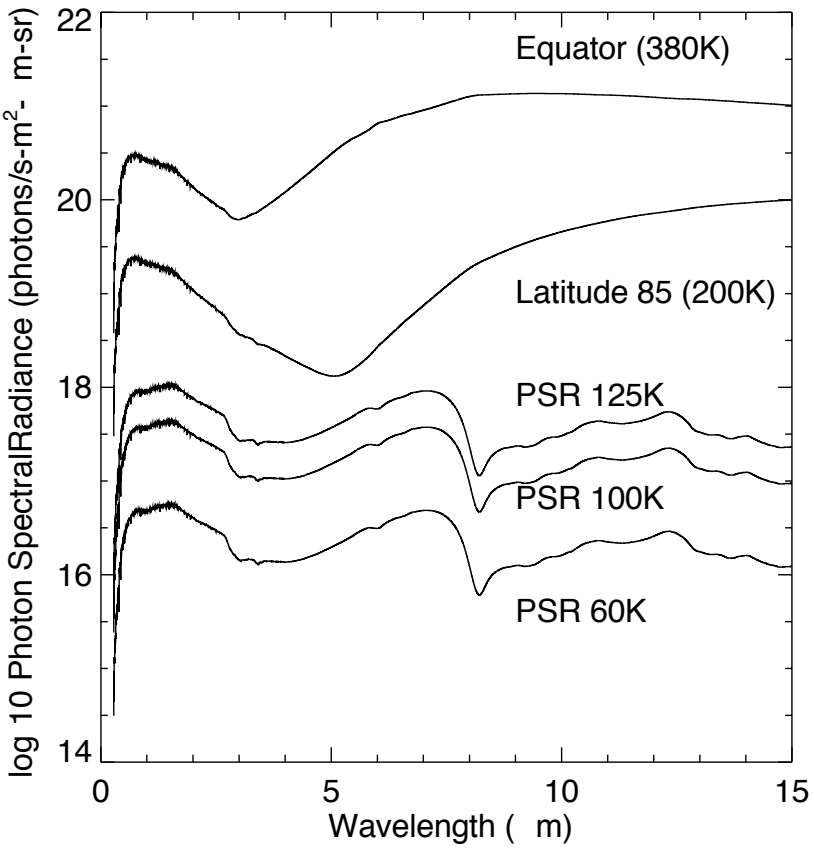

Figure 7: Same data as in Figure 6, but in units of photon spectral radiance (photons/s-m2-um-sr). Because the number of photons per watt increases with wavelength, the curves have flattened somewhat and within SPR there is almost as much signal at 7 microns as there is in the visible.

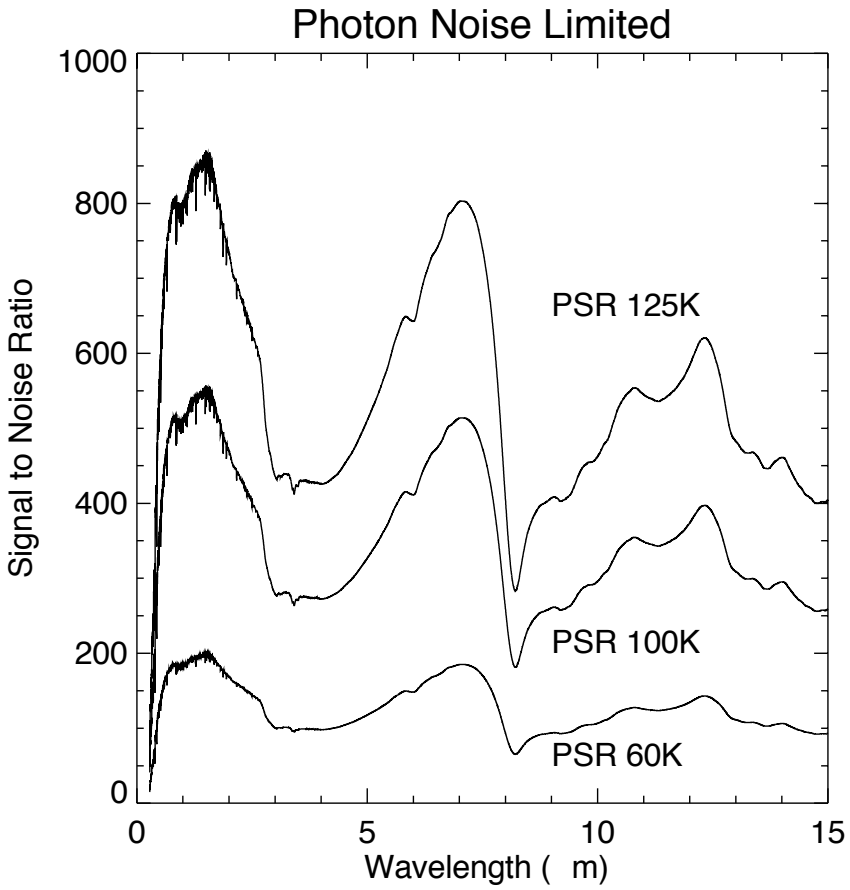

Figure 8: Signal to noise ratios of a nominal spectral sensor derived from photon radiance shown in Figure 8. The signal to noise ratios assume dominance by source photo noise and do not include read noise, dark current, sensor self emission or other noise sources. Signal to noise ratios exceed 100 even for PSR surfaces at 60K, sufficient to detect small quantities of water and other ices.

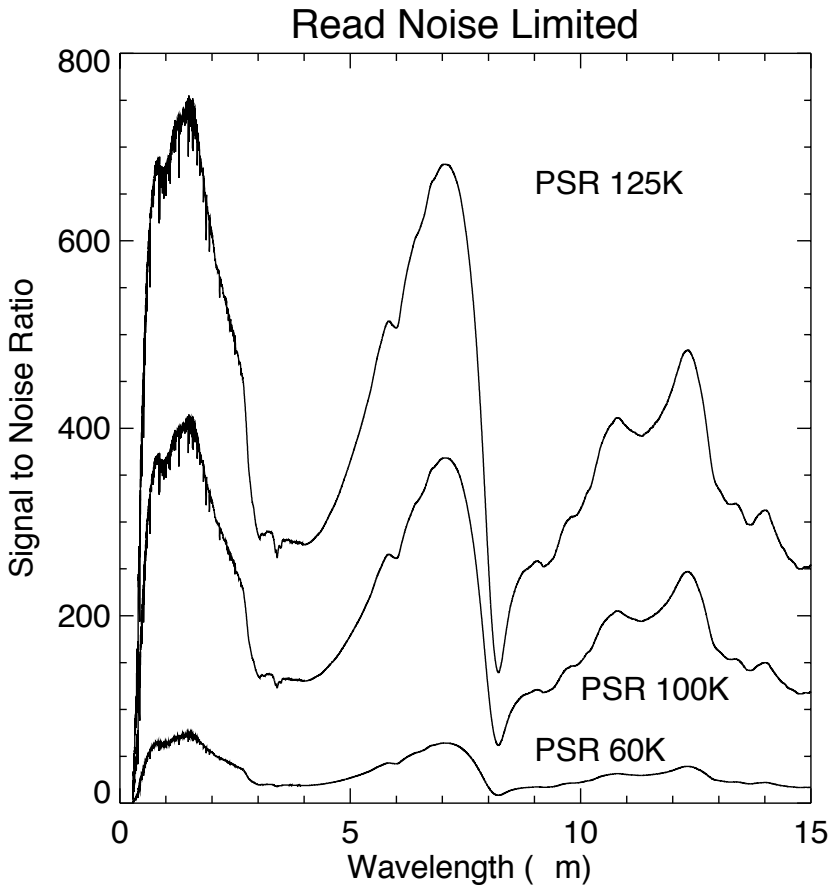

Figure 9: Signal to noise ratios including 500 electrons of read noise, which is reasonable for typical readout integrated circuits used in many IR arrays for planetary exploration. Signal to noise ratios for the warmer PSR are still quite usable, but in the coldest of the abundant PSRs near 60K are SNRs are below 30 between 3 and 5 microns, leaving little sensitivity margin.

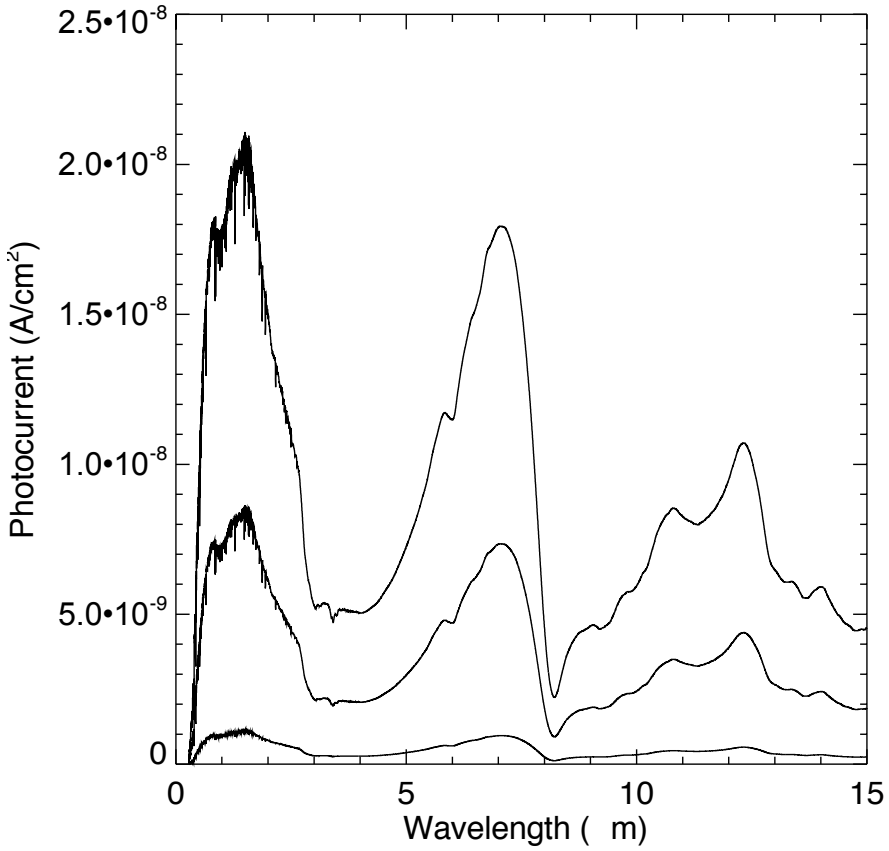

Figure 10: Photocurrent produced by the notional spectrometer described in the text when viewing the radiances shown in Figures 6 and 7. This photocurrent establishes the permissible dark current to prevent noise dominance by dark current. Our rule of thumb is that the dark current should be 1/10 the photocurrent of the lowest signal in the wavelengths of interest.

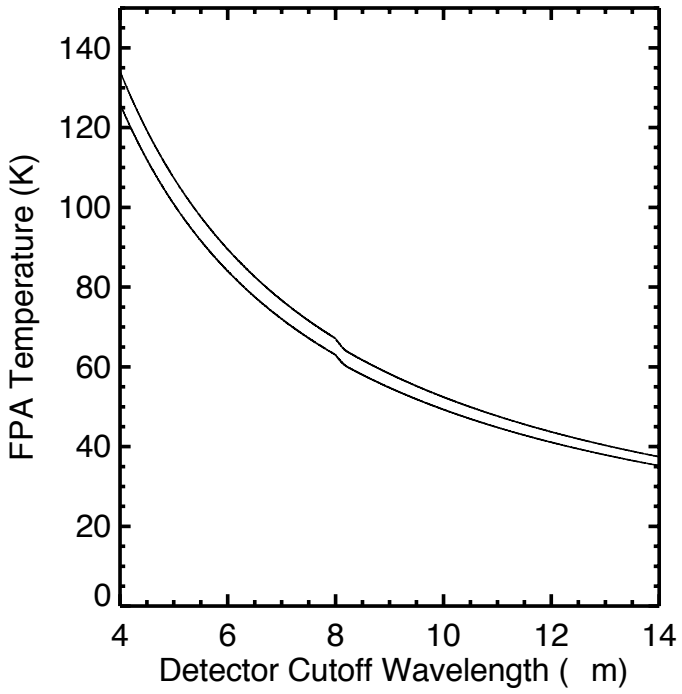

Figure 11: Focal plane array temperature required to meet the dark current requirement described in the text, for the notional spectrometer, as a function of detector cutoff wavelength. The steep decrease in temperture is due to the exponential dependence of dark current on temperature in semiconductor detectors. The top curve is for the radiance available from a 100K PSR surface and the bottom curve is for the 60K PSR surface. The difference between the curves is about 20K.

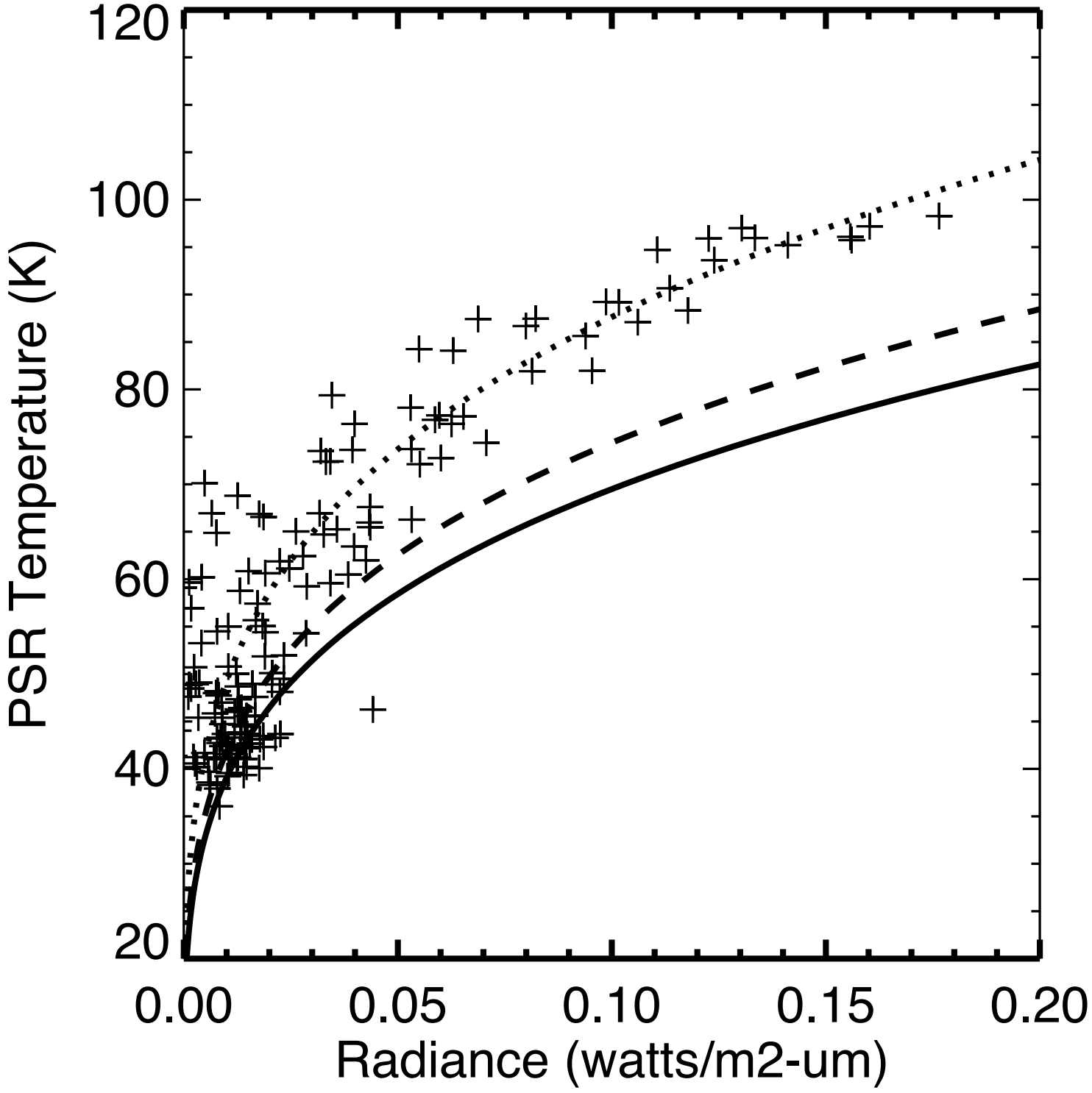
120
100
80
60
40
20
PSR Temperature (K)
0.00
0.05
0.10
0.15
0.20
Radiance (watts/m2-um)

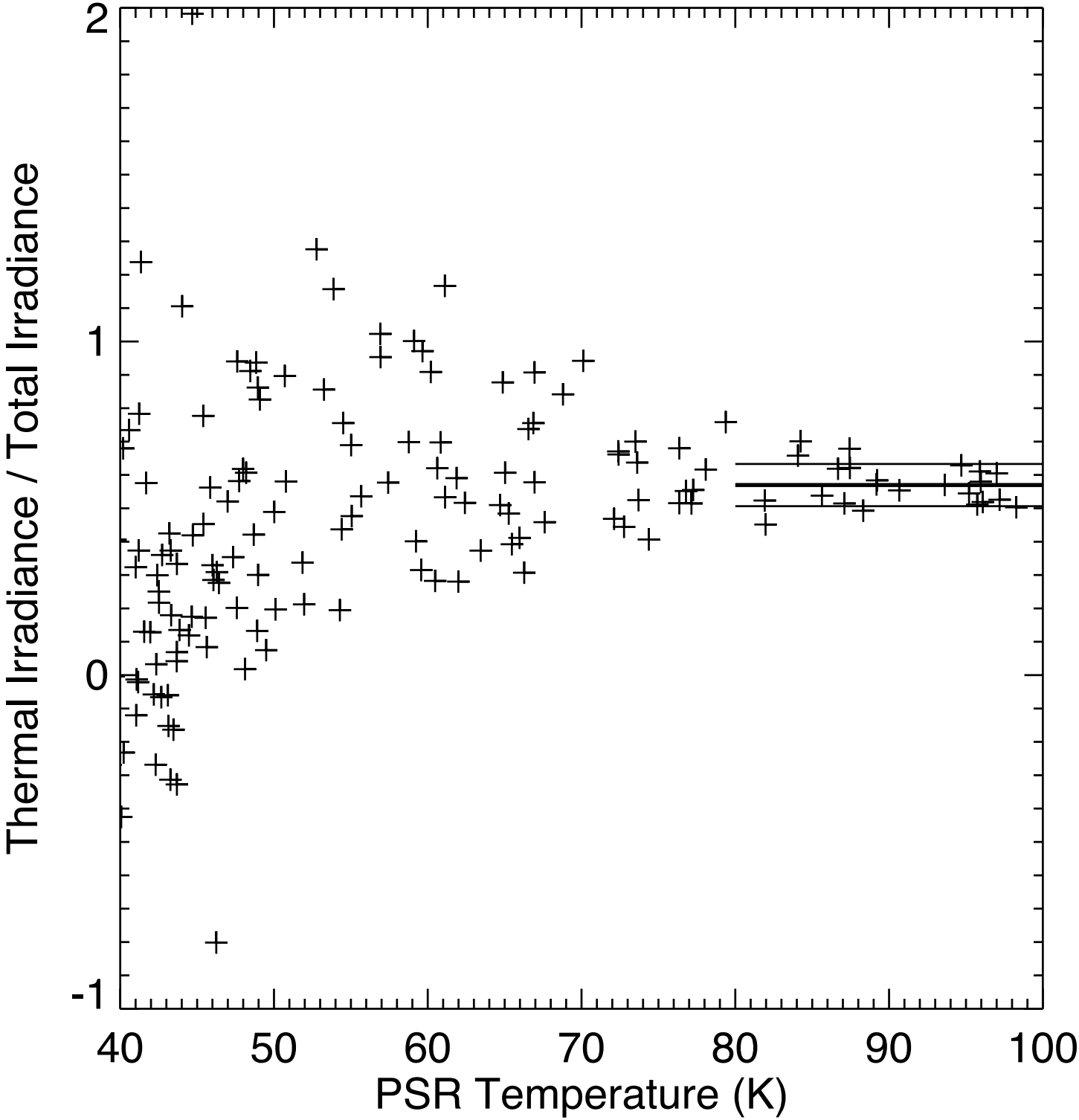
Thermal Irradiance / Total Irradiance
2
1
0
-1
40
50
60
70
80
90
100
PSR Temperature (K)

a.

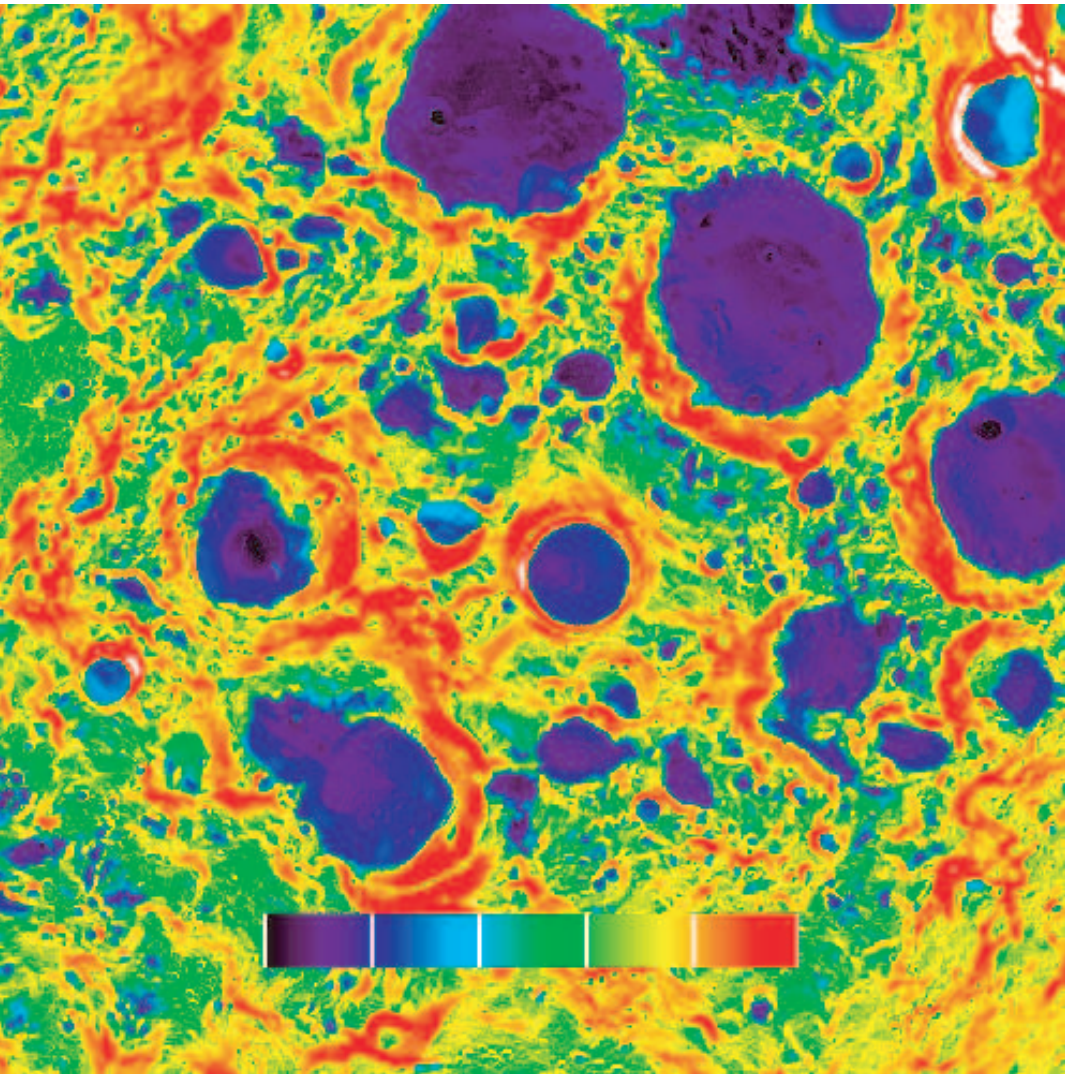

b.

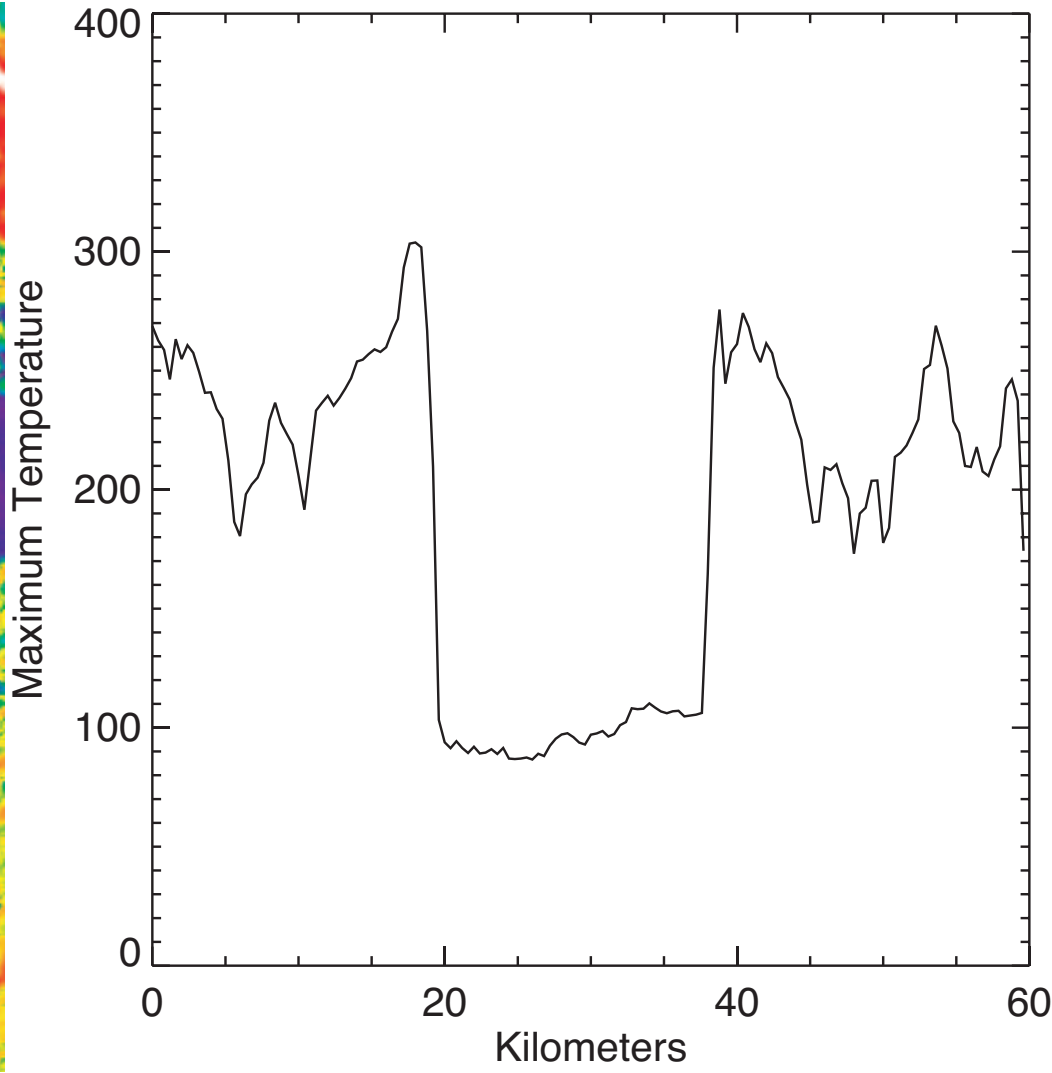

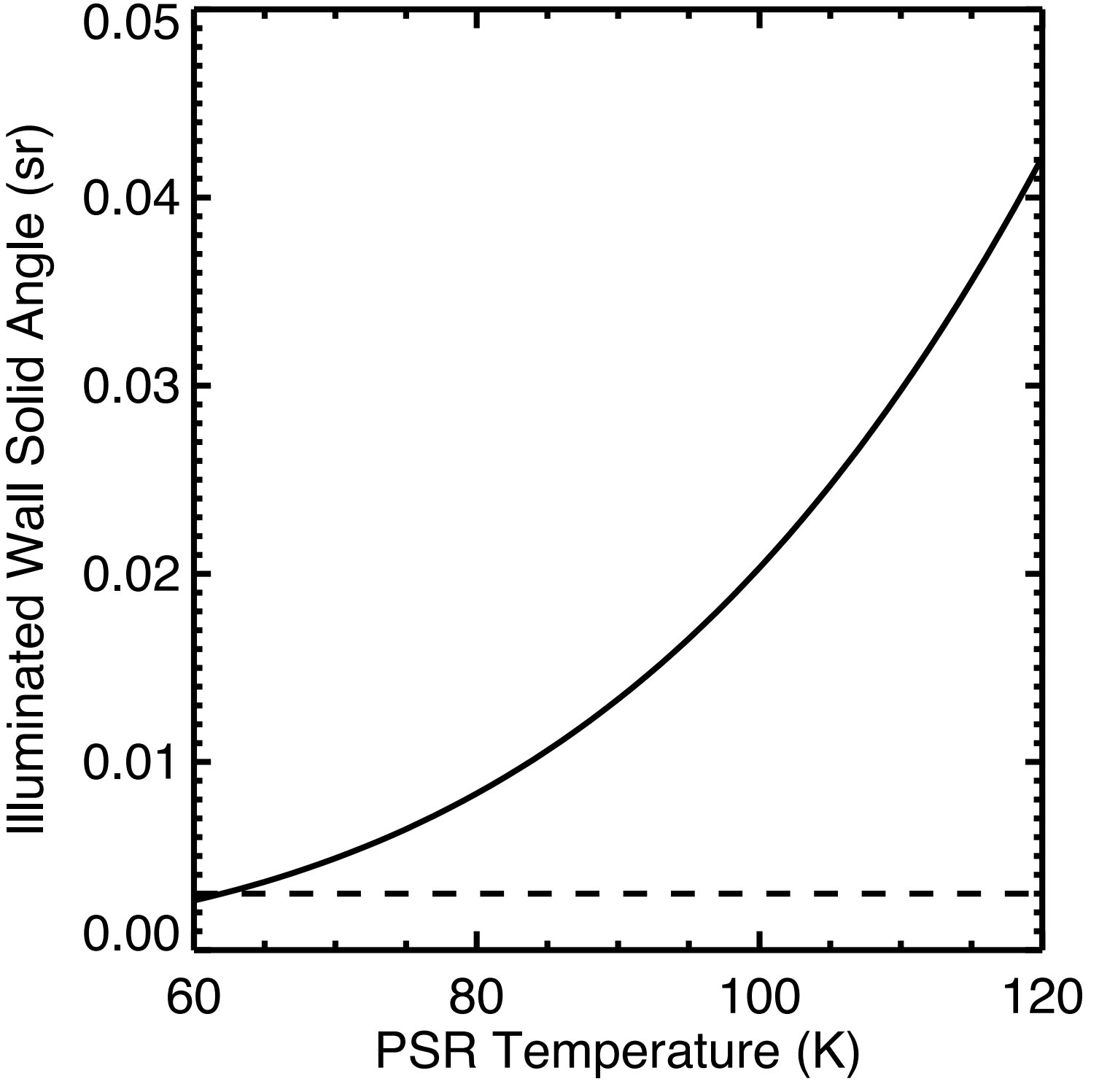
0.05
0.04
0.03
0.02
0.01
0.00
Illuminated Wall Solid Angle (sr)
60
80
100
120
PSR Temperature (K)

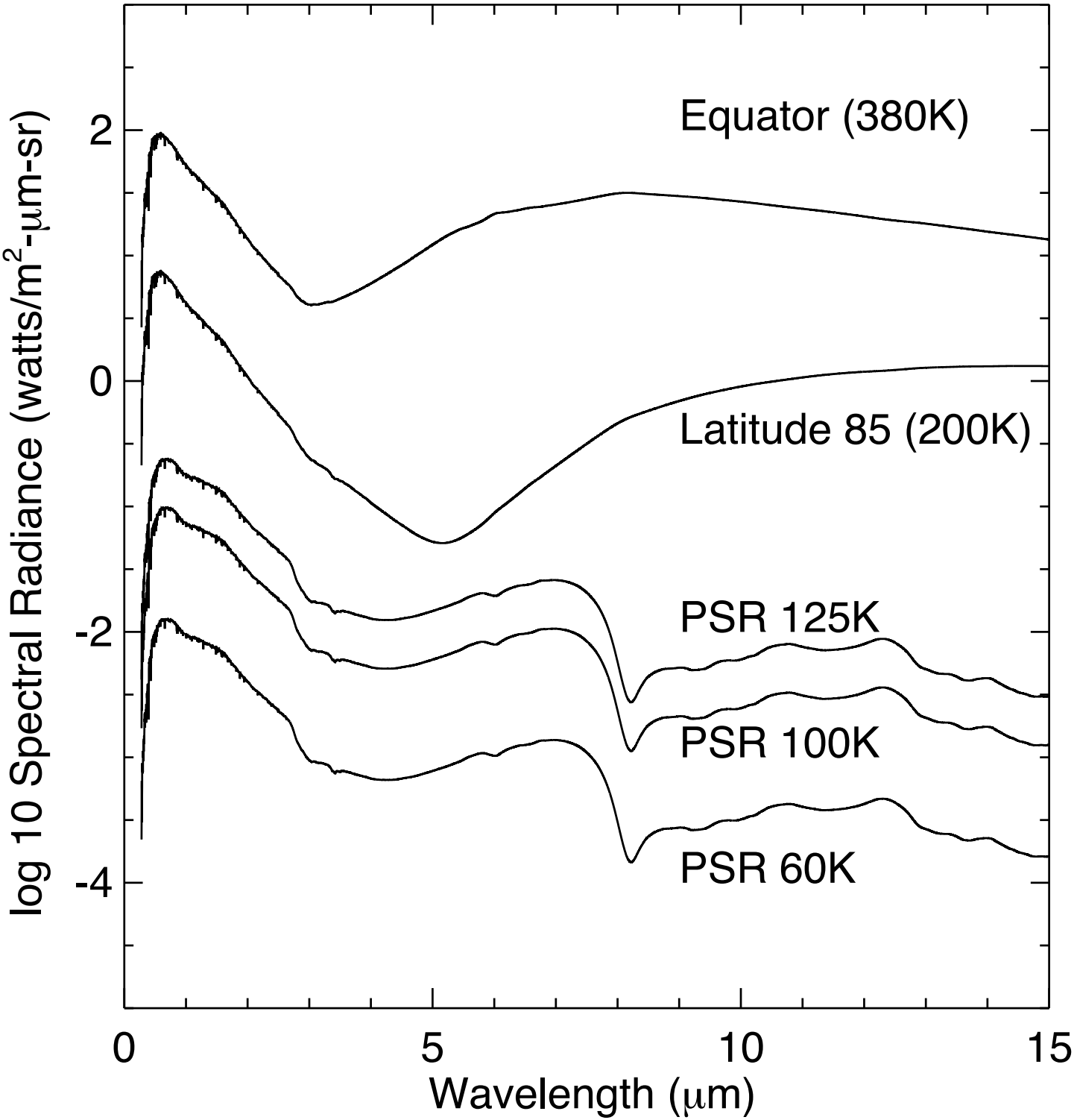
Equator (380K)
Latitude 85 (200K)
PSR 125K
PSR 100K
PSR 60K
log 10 Spectral Radiance (watts/m2-μm-sr)
2
0
-2
-4
0
5
10
15
Wavelength (μm)

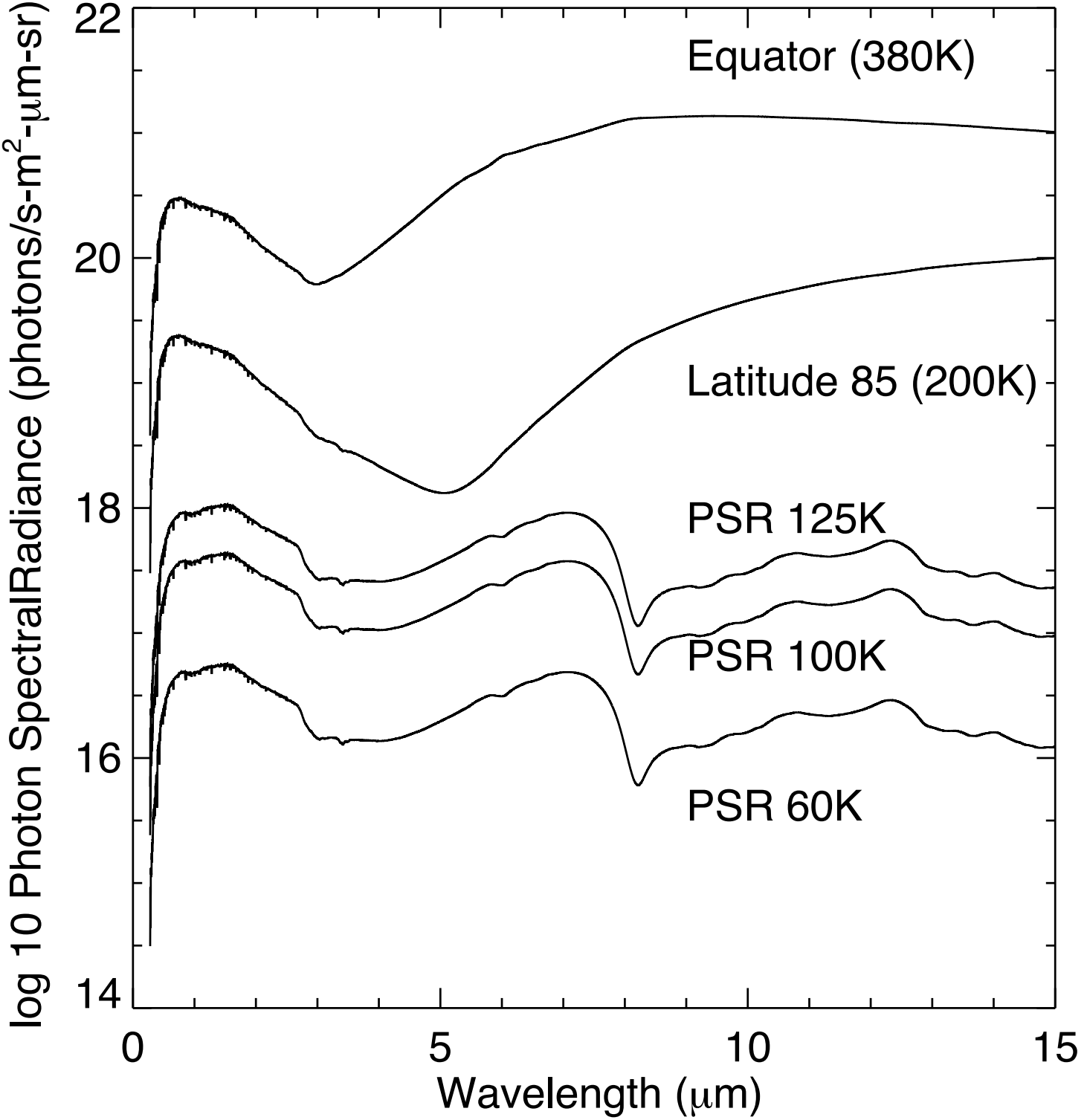
Equator (380K)
Latitude 85 (200K)
PSR 125K
PSR 100K
PSR 60K
log 10 Photon SpectralRadiance (photons/s-m^2-μm-sr)
Wavelength (μm)
22
20
18
16
14
0
5
10
15

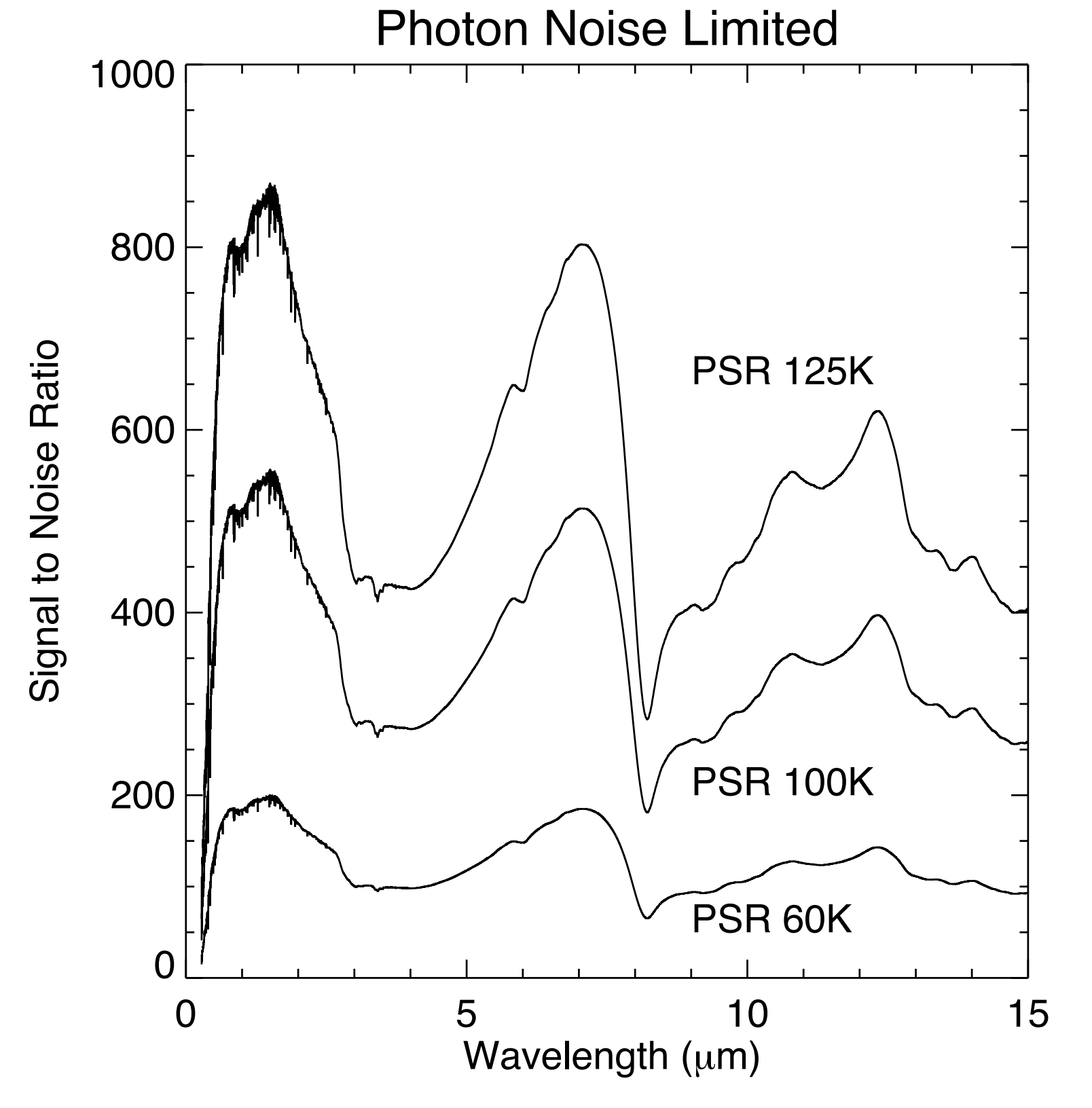
Photon Noise Limited
Signal to Noise Ratio
Wavelength (μm)
PSR 125K
PSR 100K
PSR 60K
0
200
400
600
800
1000
0
5
10
15

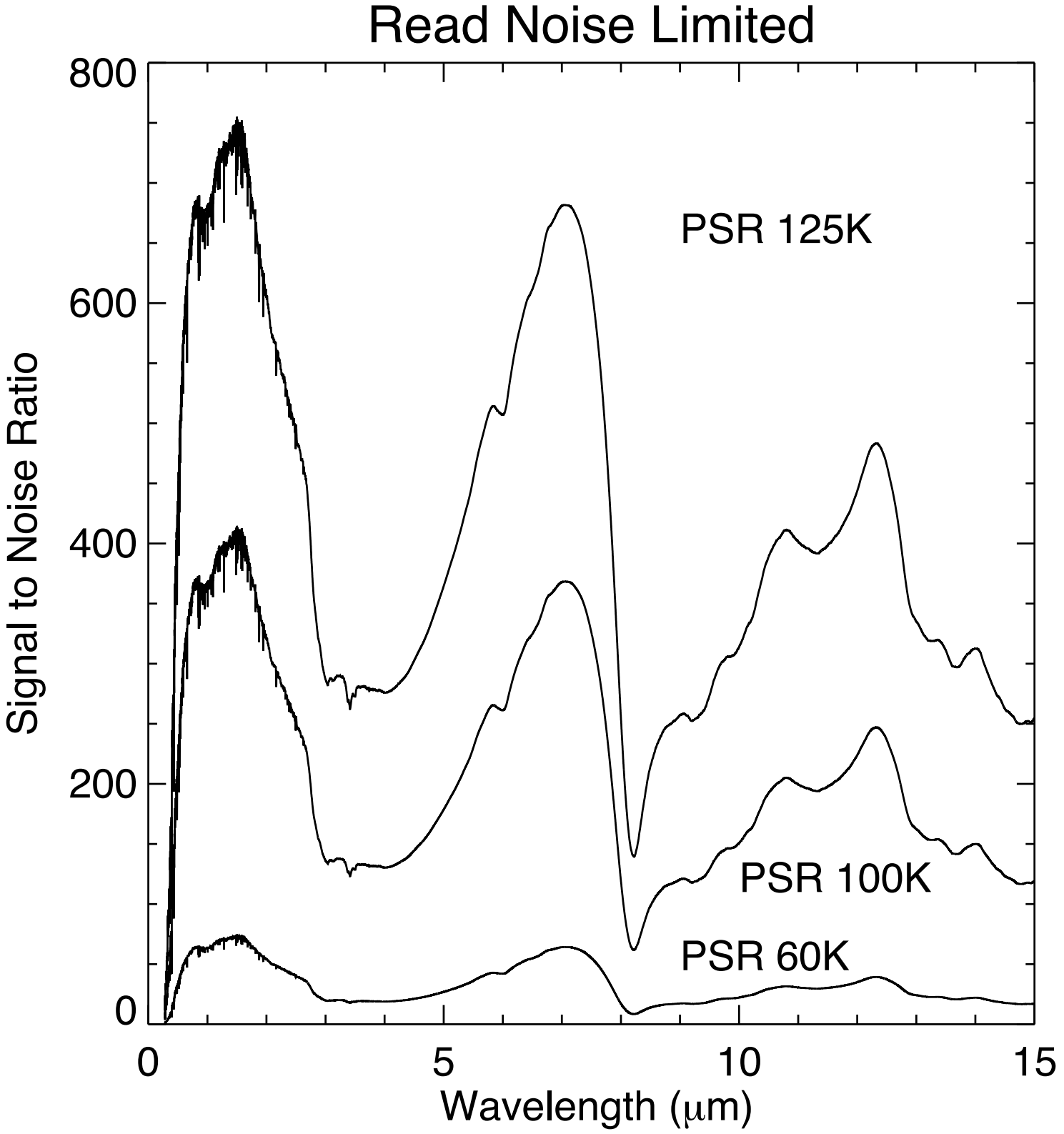
Read Noise Limited
800
600
400
200
0
Signal to Noise Ratio
PSR 125K
PSR 100K
PSR 60K
0
5
10
15
Wavelength (μm)

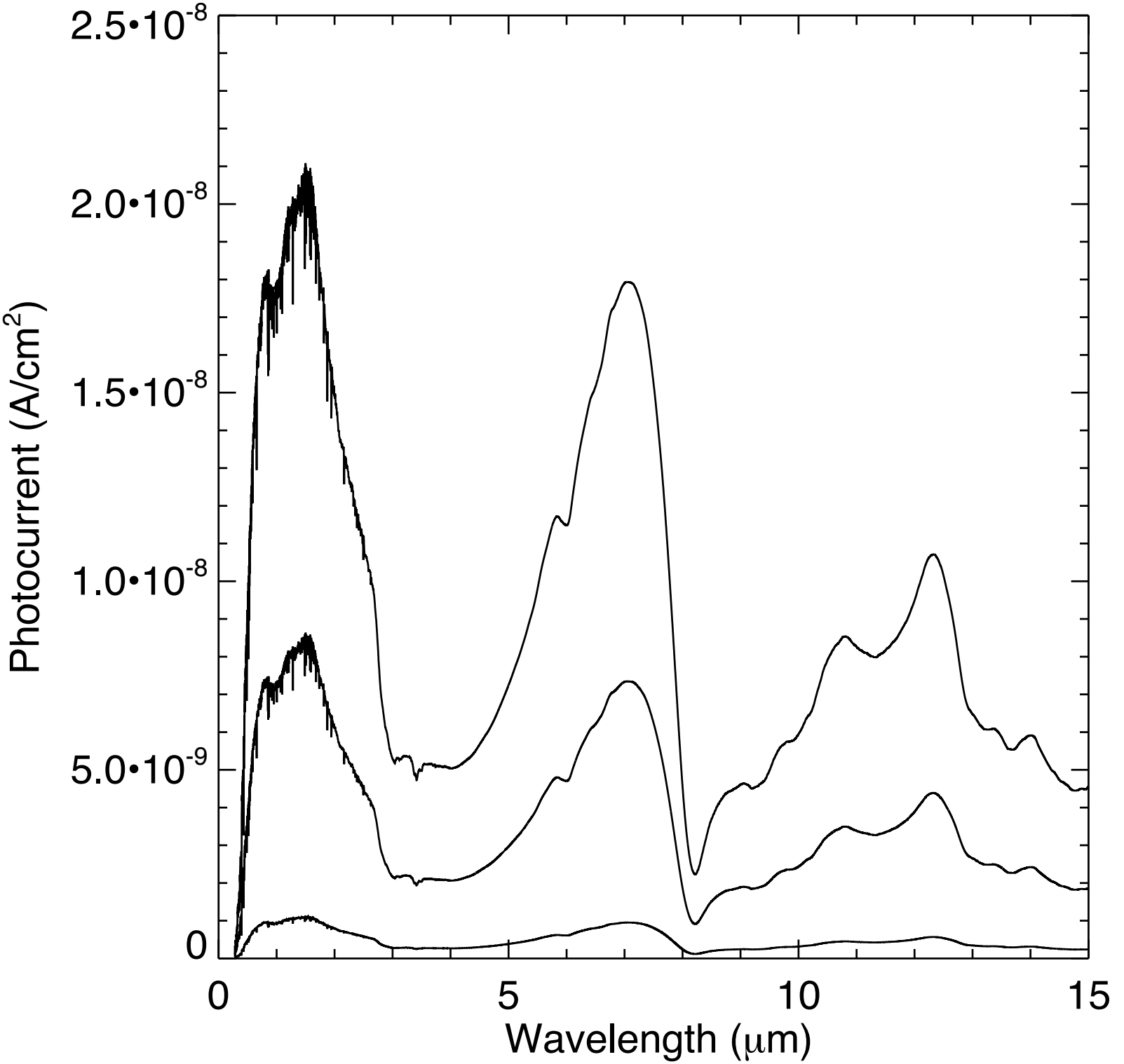
2.5•10-8
2.0•10-8
1.5•10-8
1.0•10-8
5.0•10-9
0
Photocurrent (A/cm2)
0
5
10
15
Wavelength (μm)

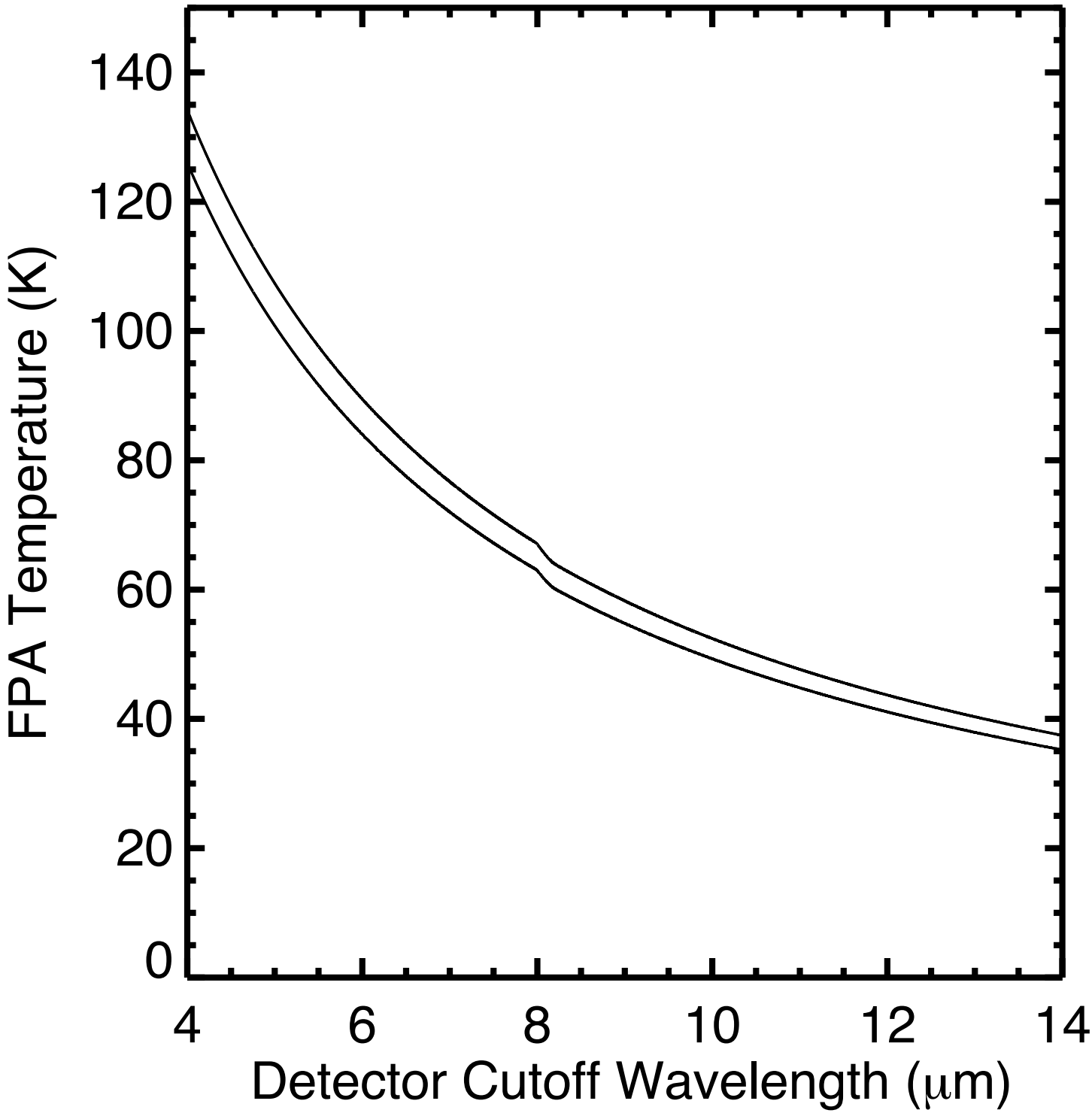
FPA Temperature (K)
140
120
100
80
60
40
20
0
4
6
8
10
12
14
Detector Cutoff Wavelength (μm)